2014

Novel 3D Head and Neck Cancer Model to Evaluate Chemotherapeutic Efficacy

Kelly Morgan
Virginia Commonwealth University

Novel 3D Head and Neck Cancer Model to Evaluate Chemotherapeutic Efficacy

by

Kelly Morgan

Thesis submitted to the Faculty of the

Virginia Commonwealth University

in partial fulfillment of the requirements for the degree of

Master of Science

in Biomedical Engineering

W. Andrew Yeudall, Chair
Gary L. Bowlin
Hu Yang
Rebecca Heise

June 2014
Richmond, Virginia

Keywords: head and neck cancer, squamous cell carcinoma, cisplatin, paclitaxel, cancer model, electrospin, 3D model, scaffold

Acknowledgments

The author wishes to thank several people. I would like to thank my primary advisor, Dr. Andrew Yeudall, for taking me on as his student and teaching me the ropes of research and how to become a master in a way that will carry through my career. I would like to thank Dr. Gary Bowlin for co-advising from the University of Memphis and helping guide me through the project. I would also like to thank Drs. Hu Yang and Rebecca Heise for the additional assistance along my research journey. I was very fortunate to work with the school of Biomedical Engineering at VCU where several opportunities opened up the door to working with the School of Dentistry, and I feel grateful for the fellow colleagues, and lab mates, that I met along the way. Lastly I would like to thank my friends and my family for helping me accomplish my goal of becoming a master, it could not have been done without their love and encouragement; especially Jarrod Chaplin for his assistance.

Table of Contents

List of Tables

Page

List of Figures

Page

Abbreviations

ANOVA	Anlaysis of variance
Bcl-2	B-cell Leukemia 2
CDDP	*cis*-diamminedichloroplatinum(II)
CMFDA	5-chloromethylfluorescein diacetate
DAPI	4',6-diamidino-2-phenylindole
DMEM	Dulbecco's Modification of Eagle's Medium
EthD-1	Ethidium homodimer-1
ECM	Extracellular matrix
FAK	Focal adhesion kinase
Tg	Glass transition temperature
H	Hill slope
HCl	Hydrochloric acid
HFP	1,1,1,3,3,3 hexafluoro-2-isopropanol
HNSCC	Head and neck squamous cell carcinomas
HPV	Human papillomavirus
Tm	Melting temperature
Taxol	Paclitaxel
Pa	Pascals
PBS	Phosphate buffered saline
PLA	Poly(lactic) Acid
PLLA	Poly(L-lactic acid)
PDLA	Poly(D-lactic acid)

S.D.	Standard Deviation
s.e.m.	Standard error of the mean
SEM	Scanning electron microscope
THF	Tetrahydrofuran
3D	Three-dimensional
2D	Two-dimensional
VEGF	Vascular endothelial growth factor
YFP	Yellow fluorescent protein

ABSTRACT

NOVEL 3D HEAD AND NECK CANCER MODELT TO EVALUATE CHEMOTHERAPEUTIC EFFICACY

Kelly Morgan, M.S.

Thesis submitted to the Faculty of the Virginia Commonwealth University in partial fulfillment of the requirements for the degree of Master of Science in Biomedical Engineering.

Virginia Commonwealth University, 2014

W. Andrew Yeudall PhD, DDS, Chair, School of Dentistry

HNSCC accounts for 7 percent of all new cancer occurrences. Despite currently available treatments, there continues to be a high mortality and recurrence rate in HNSCC. Well over 50 percent of all cancer patients receive chemotherapy as a standard treatment. However, only 5 percent of these cases have been shown to help with treatment of the disease. Formerly, two options were available for drug testing: *in vivo* animal models, and *in vitro* two-dimensional models. While *in vivo* models remain the most representative, their use is burdened by high costs, time constraints, and ethical concerns. 2D models are simple to use and cost effective, although they have been shown to produce inaccurate data regarding chemotherapeutic drug resistance due to their 2D arrangement and altered gene expression. Researchers for the past decade have been working to create 3D models that more accurately represent *in vivo* systems in order to evaluate chemotherapeutic efficacy and improve clinical outcomes. In line with this

agenda, novel 3D head and neck cancer models were created out of electrospun synthetic polymers seeded with either HN6 or HN12 cancer cells. The models were then treated with chemotherapeutic drugs (either paclitaxel or cisplatin), and, after 72 hours, subjected to a live-dead assay in order to determine the cytotoxic effects of the drugs. 2D cultures of HN6 and HN12 were also and subject to a WST-1 assay after 72 hours. The results of the treated-scaffold assays were then compared to the results of the 2D culture assays, and, as predicted, the cancer cells in a 3D culture system proved to be more resistant to chemotherapeutic drugs.

The underlying assumption for this study being that a 3D culture system based on precisely defined structural parameters would provide a practical environment to screen therapeutics for anti-cancer efficacy. To prove this, 3D scaffolds of three different fiber sizes were developed by electrospinning different concentrations of Poly(L-lactic acid) ("PLLA") (55mg/ml, 115mg/ml, and 180mg/ml) onto a mandrel that was perforated to allow for increased porosity. The resultant small, medium, and large scaffolds were then subjected to concentrated hydrochloric acid (HCl) pretreatment in order to make them less hydrophobic. Different fiber diameters represented different ECM environments for both HN6 and HN12. It was proven that both cell types thrived best in small fibers (55mg/ml-115mg/ml) than in large fibers. It was also reaffirmed through live-dead anlaysis of cells seeded on 3D scaffolds and treated with IC_{90} values of cisplatin that the head and neck cancer cells were more resistant which is more representative to the 3D environment of cancer cells *in vivo*.

Chapter 1

Introduction

1.1. Background

Annually, 650,000 people worldwide are newly diagnosed with head and neck cancer. In the United States alone there were over 39,000 new cases of head and neck cancer and over 13,000 deaths attributed to this disease in 2005. Cancers of the head and neck include cancers of the oral cavity, pharynx, larynx, salivary glands, and nose/nasal passages. Malignancies of the different cancers vary in terms of pathology and locations within the head and neck [1].

Mortality rates due to head and neck cancers have remained constant over several decades. Despite advances in delivery of treatment and surgical reconstruction, mortality rates for this disease have not improved in the past 40 years. Standard therapy today includes: radiation, surgery, and/or chemotherapy. Five year survival rate is only about 40%, primarily due to metastasis [2]. Over time, head and neck cancers will metastasize. In other words, they will disseminate and colonize organs distinct from where they originated [3]. Cancers of the head and neck tend to metastasize to nearby lymph nodes, from where the cancer cells may travel to distant sites such as the lung and the liver.

Although there are a tremendous variety of malignant processes involved in head and neck cancers, over 90% of these cancers are squamous cell carcinomas (HNSCC) [2]. Squamous cells are thin, flat cells that form the surface of the eye, skin, various internal organs, the lining of hollow organs and ducts of some glands. Head and neck cancers usually begin in the squamous cells that line the moist, mucosal surfaces in the head and neck such as the nose, mouth, and throat [4].

1.2. Prevention

There are several causes attributed to HNSCC, but the strongest risk factors are alcohol and tobacco usage. At least 75 percent of all head and neck cancers are caused by tobacco and alcohol, especially cancers of the oral cavity, oropharynx, hypopharynx, and larynx. Non-smokers and patients that drink little to no alcohol that have HNSCC may have, in some cases, been infected with cancer-causing types of human papillomavirus (HPV), especially HPV-16, particularly with cancers within the oropharyngeal region that involve the tonsils or the base of the tongue. Incidences of oropharyngeal cancers caused by HPV have been increasing in the United States [4].

Prevention of HNSCC is an important focus, so that drastic treatment measures can be avoided. Prevention can be divided into primary, secondary, and tertiary prevention. Primary prevention is cessation or avoidance of risk factor exposure such as alcohol and tobacco via education. Secondary prevention is early detection, or seeking a physician as soon as there are any differences in health. The tertiary prevention would be the reduction of complications, reducing the chance of further dysfunction including speech, dental, and swallowing problems [5].

Primary prevention is the most effective way to avoid HNSCC because it targets the risk factors that cause cancers of the head and neck. Avoiding these risk factors is an important way to avoid HNSCC altogether. Extrinsic factors include external agents such as tobacco, alcohol, dietary, sunlight, and HPV. Intrinsic factors are underlying circumstances that may predispose individuals to develop this malignancy. These intrinsic factors include immune deficiency, iron-deficiency anemia, and other genetic factors. The main way to avert HNSCC is the prevention or cessation of tobacco. Epidemiologic studies have shown that those who smoke cigarettes are

five to nine times more likely to develop oral cancer than nonsmokers; whereas this risk can increase to as high as 17 times for extremely heavy smokers [17].

1.3. Treatment

The current most common modalities for treating HNSCC are surgical excision, radiation therapy, and chemotherapy, or combinations thereof. The location, stage, size, involvement of adjacent normal structures, and the available expertise all determine the modality or combination of treatments that should be used to treat HNSCC. Considering the head and neck are the most visible and noticeable portions of the human body, treatment options are considered thoroughly. Head and neck tumors have a profound effect on the daily life of patients when it comes to speech and swallowing. Thus, the goal in treating these tumors is not only to cure the underlying malignancy but to do so with minimal effect on both function and aesthetics, in order to sustain the quality of life of the patient. In order to achieve this goal, the standard treatment today is commonly a combination of radiation therapy and chemotherapy, as opposed to the severity of excision [1]. Radiotherapy and surgical techniques have resulted in an improved survival rate, although recurrence rates have remained high, necessitating other forms of treatment [6].

1.3.1. SURGICAL EXCISION

Surgery for oral cavity and oropharyngeal cancers entails several different types of operations depending on the stage of cancer and where it is located. These surgeries include: tumor resection (removal of entire tumor), Mohs micrographic surgery (cancers of the lip), glossectomy (removal of the tongue), mandibulectomy (removal of the jaw bone), maxillectomy (removal of hard palate), laryngectomy, neck dissection, dental extraction and implants, and finally reconstructive surgery is frequently needed to restore structure or function of affected areas. Surgery contains many risks including but not limited to blood clots, infections,

complications from anesthesia, pneumonia and death. The complications vary depending on the complexity of the procedure, but regardless, the patient will experience pain afterward that is primarily treated through medication. In cancers of the head and neck, it is more common for the surgeries to be complex because the tumors may be large or strenuous to reach. In these complex surgeries several side effects can occur including wound breakdown, infection, difficulty with eating and speaking, disfiguring of anatomy, or even death during or shortly after the procedure [7].

1.3.2. RADIATION THERAPY

Radiation therapy is a minimally invasive alternative to the severity of surgical excision of tumors. Radiation therapy uses high-energy x-rays or particles to slow the growth rate or to destroy cancer cells. It has several different uses when associated with oral and oropharyngeal cancers. Radiation therapy can be used as the main treatment for small cancers. Patients with larger cancers may require the combination of surgery and radiation therapy. Post-surgery radiation therapy can be used as an adjuvant (additional treatment) in order to kill any small remnants of cancer that may have not been removed during surgery. Radiation therapy can also be used as a neoadjuvant treatment, or before surgery, to shrink tumors. Additionally, radiation therapy has been successful in cases to relieve pain, bleeding, swallowing difficulties, and metastases. Any of these cases may require the merging of radiation therapy and chemotherapy. Radiation of the mouth and throat can cause several side effects including pigment changes of the skin, hoarseness of the voice, loss in sense of taste, and redness or soreness of the mouth and throat (mucositis). Fortunately, the previously listed side effects are commonly in existence for a short period of time. Such side effects are normally more severe in patients that are receiving chemotherapy simultaneously [7].

1.3.3. CHEMOTHERAPY

It is desirable to treat HNSCC with minimal invasiveness, to sustain the quality of life of the patient. Considering the severity of the common modalities used to treat HNSCC, chemotherapy is a justifiable option. Chemotherapy is the use of anti-cancer drugs taken orally or given intravenously. There are a few different scenarios where chemotherapy may be used, including in combination with radiation therapy or surgery, or as a substitute for surgery as the main treatment for some cancers. Adjuvant chemotherapy is the combination of chemotherapeutic drugs with radiation therapy post-surgery, in order to kill any remaining cancer cells. Neoadjuvant or induction chemotherapy refers to the use of chemotherapy drugs (sometimes with radiation) to shrink larger cancers prior to surgery. This can lead to a less radical surgery and a decrease in serious surgical side effects. Last, chemotherapy may be used to treat cancers that are too large and have metastasized too widely to be removed by surgery. In this case, the drug is used to slow the growth of the cancer and help relieve any symptoms the cancer may be causing [7].

The primary goal of chemotherapy drugs is to attack cells that are dividing quickly, which is why they work effectively against cancer cells. However, other cells in the body that also divide quickly may be affected, such as bone marrow, the lining mucosa of the mouth and intestines, and hair follicles. Because of this, several side effects are attributable to chemotherapeutics. Side effects include mouth ulcers, hair loss, nausea and vomiting, a decrease in appetite, diarrhea, and a low blood count due to effects on the bone marrow. Low blood counts can lead to increased risk of infections, easy bleeding or bruising, and fatigue. Many, if not all, of these side effects improve once treatment is stopped [7].

1.3.4. FREQUENT FAILURE OF CHEMOTHERAPY

Well over 50 percent of all cancer patients receive chemotherapy as a standard treatment. However, only 5 percent of these cases have been shown to help with treatment of the disease. Chemotherapeutic drugs have been found to be highly successful in eliminating some cancer types. However, an increase in survival rates for the majority of cancer patients through chemotherapy has not been proven. Chemotherapeutic drugs are effective in killing cancer cells; unfortunately the drugs are simultaneously killing healthy normal cells. Killing of healthy normal cells results in a depressed immune system causing the cancer patients to be susceptible to several other ailments, as previously mentioned. It is true that chemotherapeutic drugs cause shrinkage in tumors, but this does not necessarily translate to long-term survival rate in patients [36].

Chemotherapy treatment can lead to death of most of the tumor cells (drug-sensitive) although some of them (drug-resistant) are able to survive and grow again. Cancer cells can develop the ability to become resistant to many different types of chemotherapeutic drugs. This process can occur through an increased efflux of drug, enhanced repair/increased tolerance to DNA damage, high antiapoptotic potential, decreased permeability, or decreased enzymatic deactivation [35].

HNSCC falls into the category of cancers that are normally unable to be treated with chemotherapy alone. As stated previously, chemotherapy is typically combined with radiation therapy, and has been reserved for those with advancement or recurrent stages of the disease. Chemotherapeutic drugs have been successfully used to control the progression of the tumor, although this treatment has not been able to translate to overall long-term survival. As mentioned formerly, survival rate for HNSCC has remained static at 40 percent for several years despite advancements in treatment [37]. Because of the failures in chemotherapy treatment, an

importance is placed on pre-testing the chemotherapeutic drugs *in vitro*. Being able to treat HNSCC *in vitro* allows for a safer setting to test the efficacy of the drug.

1.4. HNSCC Models

Cancer is considered to result from the accumulation of multiple genetic aberrations that transform cells, permitting their abnormal growth, proliferation, and metastasis. In order to research the complexity of the disease, representative cancer models are simulated in a laboratory setting. Multiple models of cancer have been described in the literature, including cancer cells in culture and genetically modified mice [8], and these have allowed significant enhancements of treatments.

1.4.1. *IN VIVO* HNSCC MODELS

In vivo models of cancer have revolutionized the ability to study gene function in cancer pathogenesis, with mice being commonly used. Mice are advantageous as a model system due to the fact that they are small in size, inexpensive to maintain, they reproduce rapidly with large litters, and are easily genetically manipulated. A mouse model may be used for several different cancer research purposes, including gene function validation, identification of novel cancer genes and tumor biomarkers, or anticancer drug testing [9].

Despite some of the limitations that may arise with *in vivo* growth of a tumor, there is no current technology or *in vitro* assay that can predict the activity of antineoplastic drugs or demonstrate the tumorigenic and metastatic properties of tumors as accurately as xenograft animal models [10]. However, the testing of animal models can become expensive, time consuming, and have ethical concerns [22].

1.4.2. *IN VITRO* HNSCC MODELS

Immortalized cell lines derived from HNSCC tumors are an *in vitro* system that enables

research into the molecular, biochemical, genetic, and immunological properties of head and neck cancer. There are several advantages when using cell culture, such as sample homogeneity, cost, and the lack of legal and ethical issues associated with animal experimentation. The process of establishing HNSCC cell lines over time has proven to be challenging due to fibroblast overgrowth, long quiescent periods before passaging the cells, and primary and secondary cultures being dependent on feeder layers. Several different technical improvements have taken place in order to make successful permanent culture of HNSCC cell lines more feasible. Therefore, more than 300 reported HNSCC cell lines have been developed, which is considerably more than cell lines derived from breast, colon, and prostate cancers [10].

Cancer cell cultures are typically grown as monolayer cells on polystyrene plastic. Although, some models introduce a three-dimensional (3D) setting for the cancer cells to grow, which more accurately represents tumor cell characteristics such as drug response or metastatic potential [10].

1.5. Cell Sources For In Vitro Models

1.5.1. EXTRACELLULAR MATRIX OF HNSCC

The macromolecules that make up the extracellular matrix (ECM) of HNSCC are primarily proteins and polysaccharides secreted locally and assembled into an organized meshwork. This meshwork of proteins and polysaccharides works closely with the surface of the cell that produces them [14]. The ECM associated with epithelial structures is mainly composed of laminin, collagen, fibronectin, and glycosaminoglycans. This was once viewed as the architectural support of the cells, but it is now understood that the ECM is a major regulator of cell activity. The molecules that make up the ECM act as ligands for integrins which, in turn, support tissue development, tissue maintenance, wound healing, and oncogenesis. Changes in

the composition of the ECM, altered expression, secretion, or processing, directly impacts oncogenic development, hyperplastic growth, and tumor development [15].

1.6. Electrospinning

Electrospinning is a commonly used technique within the field of tissue engineering. The process of electrospinning allows for the engineering of 3D scaffolds that can support cell growth and proliferation. Electrospinning is an attractive technique for nanofiber fabrication which can be used to produce fibers ranging from several micrometers to about 100 nm or less. Several different natural substances are able to be electrospun such as collagen, silk fibroin, chitosan, gelatin, and a wide range of biodegradable polymers [28]. Electrospun scaffolds are used as a framework for host cells to populate and deposit ECM components to eventually replace the targeted organ [16]. The host-appropriate cells are then able to proliferate and occupy the void spaces with their own extracellular matrices within the scaffold. With the process of electrospinning, properties of the engineered scaffold are able to be manipulated for ideal cell viability, proliferation, migration, and differentiation. Some key characteristics of an ideal scaffold are appropriate levels and sizes of porosity for cell migration; sufficient surface area and surface chemistries to encourage cell adhesion, growth, migration, and differentiation; and a degradation rate that closely matches the regeneration rate of the desired natural tissue [16].

Electrospinning is a mesh of synthetic or natural material consisting of fibers with ranging diameters. These materials are biocompatible in order to eliminate concerns regarding unfavorable immune responses or disease transmission. The principal elements needed for electrospinning are a polymer source, a high voltage supply, and a collector. With the input of the high voltage supply, an electric potential occurs between the polymer source and the collector. Charge then accumulates and is forced to the surface of an emerging polymeric droplet, through a syringe connected to a pump, at the end of a metal needle. The force of the electric field becomes larger than the cohesive force of the solution, which is predominantly surface tension, and an electrically charged jet of polymer containing solution erupts. This jet then migrates towards the collector plate and is elongated by electrostatic interactions between charges on nearby segments of the same jet. Through this electrostatic migration, the solvent evaporates and the jet solidifies into a fiber as can be seen in Figure 1.1 [16].

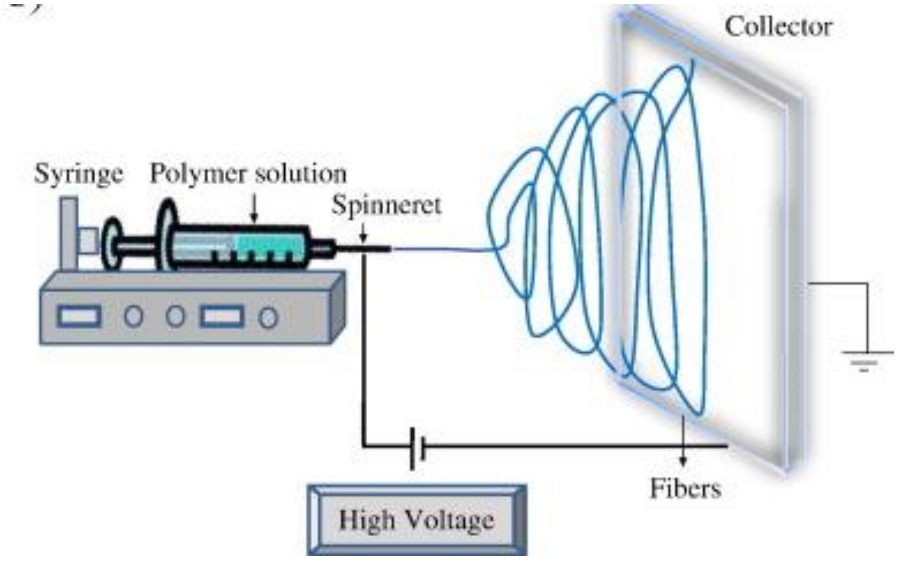

Figure 1.1: Schematic diagram of set up of electrospinning apparatus [38].

It is advantageous to fabricate a synthetic ECM through tissue engineering because it is chemically pure. In other words, the ECM contains no uncharacterized growth factors or other contaminants when made with synthetic material, such as Polylactic Acid (PLA), which makes

the scaffold easy to engineer chemically. This provides the possibility for elegant cross-linking and multiple modification options, which allows the scaffold to be used in a variety of ways such as artificial tissues, surgical devices (sutures, clamps, etc.), drug delivery devices, and drug testing models. The main disadvantage of synthetic matrices is that they are not as biologically relevant as naturally derived matrices therefore they may not contain the signaling molecules and sequences that native ECM provides [22].

In the field of tissue engineering, bio mimicry has been the major impetus for biomedical applications. Since the natural ECM is composed of fibrillar collagens that are approximately 50 to 150 nm in diameter, biomimicking similar features has led to the engineering of nanoscaffolds of the same dimensional scale. Studies have shown that nano-dimensional surfaces on tissue engineered scaffolds lead to enhanced cell adhesion and proliferation over micro-dimensional surfaces. It has also been shown that cells organize well around fibers with diameters smaller than the diameter of the cells. Better cell attachment occurs in smaller diameter scaffolds, as it is thought that the smaller surface area localizes more absorption of adhesion proteins. Smaller fiber diameters have been found to have a higher cell growth rate because of larger surface area-to-volume ratio that allows for more cell growth factors to bind to the fibers. It is also possible that scaffolds with smaller diameters are more pliable, which allows cells to migrate within the scaffold with less force [28].

1.6.1. POLY(LACTIC) ACID

Poly(lactic) acid (PLA) is known as one of the most promising biodegradable polymers used for commodity applications. PLA is a thermoplastic, aliphatic polymer that is derived from renewable resources such as corn starch and sugar cane via fermentation and ring-opening polymerization. The biodegradability and biocompatibility of PLA are sufficient enough for the

polymer to have been used for three decades in biomedical applications. PLA has been used in biomedical devices including sutures, clips, tissue engineering scaffolds, and drug delivery devices [20]. With breakthroughs in biotechnology, within the past decade high quality PLA has been able to be mass-produced and commercialized for targeted, low-cost fiber, insulation, and packaging applications. Other than the drive of cost, PLA is a desired polymer in biomedical applications because of the ability to tailor its physical properties. The physical properties that are able to be modulated in PLA are molecular weight, molecular topology, and mixing ratio of three stereoisomers, L-lactide, D-lactide, and meso-lactide, during synthesis [18].

One drawback of PLA is that its degradation rate through hydrolysis can be very slow, which may be detrimental for biomedical purposes. The polymer is also very brittle, with less than 10 percent elongation at break, which makes PLA unsuitable for demanding mechanical performance applications. The most unfavorable quality of PLA when it comes to tissue engineering is its strong hydrophobicity. Because of its strong hydrophobicity, PLA can elicit an inflammatory response from host tissues, which in turn educes a low affinity with cells when using tissue engineering materials [20].

1.6.2. POLY(L-LACTIC ACID)

As discussed previously, PLA is derived from lactic acid that exists as two enantiomers: L- and D-lactic acid (PLLA and PDLA, respectively). The degradation rate half life of PLLA is about six months to two years [20]. Specifically, PLLA is used similarly to PLA for several tissue engineering procedures. Table 1.1 shows the variations between the different physical and chemical properties of PLA. PLLA is a semicrystalline polymer, where crystal polymorphism has been studied extensively because mechanical properties of the polymer depend heavily on crystal structure [19].

Table 1.1 Selected physical and chemical properties of PLLA [20].

Properties	PDLA	PLLA	PDLLA
Solubility	All are soluble in benzene, chloroform, acetonitrile, tetrahydrofuran (THF), dioxane etc., but insoluble in ethanol, methanol, and aliphatic hydrocarbons		
Crystalline structure	Crystalline	Hemicrystalline	Amorphous
Melting temperature (Tm)/ °C	~180	~180	Variable
Glass transition temperature (Tg)/ °C	50-60	55-60	Variable
Decomposition temperature/°C	~200	~200	185-200
Elongation at break/ (%)	20-30	20-30	Variable
Breaking strength/ (g/d)	4.0-5.0	5.0-6.0	Variable
Half-life in 37°C normal saline	4-6 months	4-6 months	2-3 months

1.6.3. MECHANICAL PROPERTIES OF BIOMATERIALS

Tissue engineering uses the method of electrospinning to produce scaffolds composed of biomaterials that mimic native tissue as much as possible. One property of great importance when considering the imitation of native tissue is the mechanical properties of the biomaterial. Mechanical properties can help mirror intrinsic characteristics of the tissues such as its crystallinity and structure of its ECM fibers. A few distinct parameters that are recognized through mechanical testing of scaffolds are strength, peak stress, strain, and Young's modulus. Strength is measured as the force applied to the scaffold over the cross-sectional area of the scaffold which is otherwise defined as stress. Strength is measured in N/m^2 or Pascals (Pa). Peak stress is the maximum amount of stress a solid material can withstand, this parameter can

conveniently be used to compare with other biomaterials. Strain is a deformation of solid material under a known stress. In short, strain is the ratio between initial shape and deformation of an object which makes strain a unit less measurement. The testing is done under a uniaxial tensile loading which causes a longitudinal deformation. The stretching is done under a known stress where the ratio between the changes in length to the final length prior to failure is determined. This uniaxial stretching is classified as stress vs. strain which is described by the numerical constant known as tensile or Young's modulus. This numerical constant describes the elastic properties of isotropic material undergoing tension or compression uniaxially. Young's modulus is a measure of the ability of a material to withstand changes in length under tension or compression and is equal to the longitudinal stress divided by the strain, within the elastic range of the material [21]. Since Young's modulus is the ratio of stress (Pa) and strain (unitless) the constant is calculated in Pa. Quantifying the information from mechanical testing biomaterials is a crucial aspect of tissue engineering. With these data, scaffolds can more efficiently be engineered to mimic, or even improve, the mechanical functions of the native tissues [6, 19].

1.7. Drug Testing in HNSCC

Traditionally, chemotherapeutic drugs have been tested on tumor cells that are cultured as two-dimensional (2D) monolayers on plastic cell culture plates. Current 2D monolayer drug testing may not accurately mimic 3D arrangements where cancer cells reside *in vivo*. Because of these artificial conditions, there are large changes in gene expression compared to tumors *in vivo* including: signal transduction, cellular movement, cell-to-cell signaling, cellular growth, and morphology. Several laboratories have reported that differential gene expression between 2D and 3D arrangements leads to inaccurate data regarding predicted responses of cancer cells to chemotherapeutics [22, 23].

The utilization of 3D cell culture models has become increasingly popular because these structures resemble *in vivo* structures with an improvement in cell-to-cell and cell-to-matrix contact. As described previously, one of the most common forms of 3D cell culture system is a prefabricated scaffold. Mechanical properties of the scaffold and the ECM of tumor cells cultured in a 3D environment affect behavior and gene expression of cancer cells. The transition from 2D to 3D has shown an elevation in chemoresistance to anticancer drugs when tested on cells cultured in a 3D model. It has been hypothesized that the 3D model allows for pro-survival signaling and an upregulation of genes conferring drug resistance and may also limit diffusion of drugs. It is also apparent that tumor cells adopt a different morphology in 2D compared with 3D, as in 3D the tumor cells are more clustered and show a more rounded shape. Studies have shown that tumor cells express different genes in 3D such as an increase in glycolytic enzymes and other key regulators. Genes that show elevated expression in 3D cancer models include vascular endothelial growth factor (VEGF) which contributes to angiogenesis, and genes responsible for cell migration and invasion including Rho GTPases and focal adhesion kinase (FAK) [22, 23]. Testing chemotherapeutics on tumor cells cultured in 3D cancer models may better recapitulate the drug sensitivity of these tumors *in vivo*. There are several chemotherapeutic drugs that are routinely used for treatment of HNSCC, but for our study we have chosen to work with two well-established chemotherapeutic drugs. Both of these drugs have been used clinically for many cancer types, including HNSCC, but have been known to elicit resistance in clinical applications [6].

1.7.1. PACLITAXEL

One of the well-established chemotherapeutic drugs chosen for this study is Paclitaxel (Taxol) [23]. Paclitaxel is an off-white crystalline powder ($C_{47}H_{51}NO_{14}$) with a molecular weight of 853.9. It is highly lipophilic, therefore insoluble in water, and melts around 216-217°C [31].

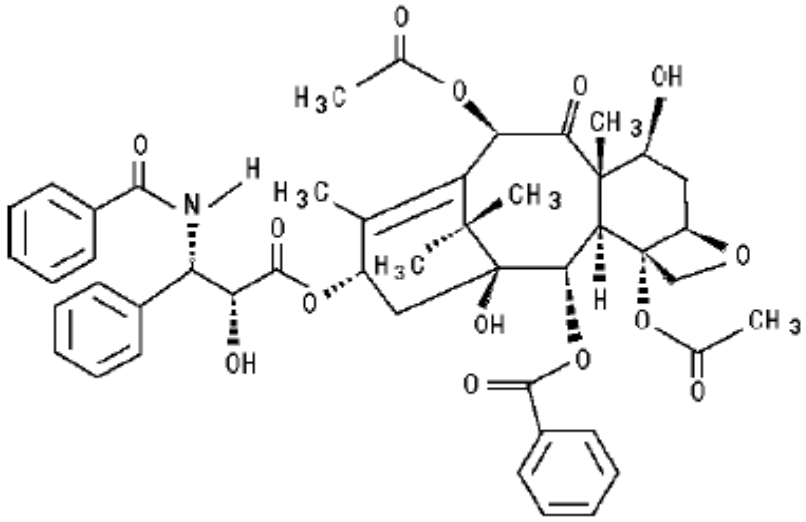

Figure 1.2: Chemical structure of Paclitaxel [31].

Paclitaxel is a compound with antineoplastic activity, inhibiting or preventing the growth and spread of tumors or malignant cells, that was extracted from the Pacific yew tree *Taxus brevifolia*. This chemotherapeutic functions by binding to tubulin and inhibits the disassembly of microtubules which in return results in the inhibition of cell division. Essentially, Paclitaxel is able to prevent depolymerization by stabilizing and rearranging the cytoskeleton of the cancer cells and arresting them in G2 or M phase of the cell cycle. This procedure causes the affected cells to either undergo apoptosis or remain in a growth-arrested state [6]. The induction of apoptosis occurs when Paclitaxel binds to and blocks the function of the apoptosis inhibitor protein Bcl-2 (B-cell Leukemia 2) [23]. According to prior studies done in this laboratory, HN12 cells cultured in 2D have been shown to be sensitive to therapeutic doses of Paclitaxel [6].

Paclitaxel has been approved to be used either alone or in combination with other drugs

to treat AIDS-related Kaposi sarcoma, breast cancer, non-small cell lung cancer, ovarian cancer, and other types of cancer including HNSCC [23]. Intravenous injection of Paclitaxel causes a large decrease in the number of white blood cells, which results in an increased susceptibility to infections. Side effects include: pain, redness, swelling around injection site, weakness, muscle or joint pain, nausea, vomiting, diarrhea, stomach pain, mouth ulcers, hair loss, numbness, burning, tingling in the hands or feet, pale skin, excessive tiredness, unusual bruising or bleeding, chest pain, slow or irregular heartbeat, fainting, and blistering or peeling skin [24].

1.7.2. CISPLATIN

Cisplatin, also known as Platinol or *cis*-diamminedichloroplatinum(II) (CDDP), is one of a series of platinum-compound chemotherapeutic drugs which are informally referred to as platins [25]. Cisplatin is an alkylating agent and attaches an alkyl group to the guanine base of DNA at the number seven N atom of the purine ring. By cross-linking the DNA, cisplatin inhibits DNA repair and DNA synthesis in cancer cells [26]. Since cancer cells have the tendency to proliferate faster with less error-correcting than healthy cells, cancer cells are considerably more sensitive to DNA damage [25].

Cisplatin is a heavy metal complex with a central atom of platinum surrounded by two chloride atoms and two ammonia molecules in the *cis* position. Cisplatin comes in a crystalline, white powder form with a molecular formula of $PtCl_2H_6N_2$ and a molecular weight of 300.05. This drug is soluble in water or saline at 1 mg/mL and dimethylformamide at 24 mg/mL with a melting point of 207°C [32**].**

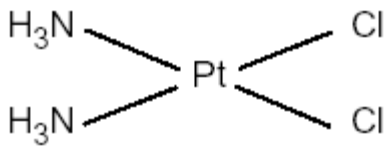

Figure 1.3: Chemical structure of Cisplatin [32].

Cisplatin has been used to treat cancers of the bladder, ovaries, testicles, and other types of cancer such as HNSCC. This chemotherapeutic drug is given intravenously for at least one hour and the dosage is dependent on the type of cancer being treated, the size of the patient, and renal health [26]. As with several other chemotherapeutics, cisplatin is potent enough to kill normal cells which can result in several side effects that may last for months or even years after medicinal use [25]. With coordination complexes of platinum, the main dose-limiting side-effects of cancer treatment are neurotoxicity and peripheral neuropathies. This results in numbness of the hands and/or feet as well as a tingling sensation in any of these extremities. Several other side effects may exist due to cisplatin including kidney damage, decreased blood levels of magnesium, potassium, and calcium, nausea, vomiting, low white blood cell count, low platelet count, increased bleeding, low red blood cell count (anemia), changes in taste, and fetal changes if pregnant [26].

1.8. Hypothesis and Specific Aims

1.8.1. HYPOTHESIS

A 3D culture system based on precisely defined structural parameters provides a practical environment to screen therapeutics for anti-cancer efficacy.

1.8.2. SPECIFIC AIMS

Specific Aim 1: Test sensitivity of HNSCC cells grown in 2D culture to cisplatin and paclitaxel.

Rationale: HNSCC accounts for 7 percent of all new cancer occurrences. Despite currently available treatments, there continues to be a high mortality and recurrence rate in HNSCC [6]. Although there have been recent advances in delivery of treatment and surgical reconstruction, mortality rates for HNSCC have not improved in the past 40 years. Currently, anti-cancer chemotherapeutics are routinely tested on 2D monolayer cell cultures. It has been shown in previous studies that tumor cells grown in 2D monolayer culture are much more sensitive to chemotherapeutic drugs [6, 27]. It is important to determine drug sensitivity of HNSCC cells in monolayer culture, so that their response in 3D environment can be investigated.

Specific Aim 2: Construct a 3D culture system of different fiber dimensions by electrospinning to test the effect of fiber diameter in cell growth and drug sensitivity.

Rationale: The field of tissue engineering has developing materials to reconstruct damaged or missing tissues or organs. Tissue engineering has not normally focused on creating tumor models for *in vitro* evaluation of drug efficacy. For this purpose, we propose to use electrospinning of PLLA to form scaffolds of three different fiber diameters: small, medium, and large. We suggest that different fiber diameters will elicit different cellular characteristics and therefore represent different 3D tumor models. From the three fiber sizes, we would be able to decide which fiber dimension would provide the best cell infiltration, cell survival, and overall drug testing apparatus.

Specific Aim 3: Test the effect of varying fiber diameter on HNSCC drug sensitivity in 3D culture.

Rationale: Several studies have shown that anticancer drugs do not work as effectively *in vivo* as they do on a 2D cell monolayer. Discrepancy in drug efficacy is due, in part, to the 3D

nature of tumors as opposed to the 2D nature of monolayer culture. It is known that cells grown in 3D have different cell surface receptor expression and proliferation, cell density, extracellular matrix synthesis, and metabolic functions than cells grown in 2D monolayer. It has been suggested that many important signals, key regulators, and tissue phenotypes are lost when cells are cultured in 2D substrates (culture plates) instead of a 3D environment. In order to more realistically assess drug efficacy prior to testing in animal models or patients, it is important to develop an *in vitro* model of a tumor that would resemble an actual tumor [26].

Different fiber diameters represent different ECM environments for the cells, including mechanical properties, porosity, possibilities for angiogenesis, along with other characteristics of the microenvironment. We hypothesize that different fiber diameters will result in differences in infiltration, migration, and adhesion of the cancer cells.

Chapter 2

Methods and Materials

2.1. Cell Culture

2.1.1. HN6, HN12, HN12-YFP CELL LINES

A model HNSCC cell line frequently used is the WSU-HN12, also known as HN12, which was established at Wayne State University in 1994. The HN12 cell line was derived from metastatic tumor from lymph nodes [6]. Over 50 studies indexed in PubMed characterize these cells as representative cells of HNSCC in a variety of drug response as well as mechanistic studies [11]. The majority of the studies were performed in 2D cultures, some of the studies included injecting the cells into nude mice representing in vivo models. Each of these studies found that HN12 cells are highly proliferative, motile, and tumorigenic *in vivo*. HN6 cell lines,

which are less commonly used, were derived from primary metastatic HNSCCs which have been described previously [48].

HN12 and HN6 cell lines were propagated in Dulbecco's Modification of Eagle's Medium (DMEM) (Life Technologies, Grand Island, NY) supplemented with 10% (v/v) fetal bovine serum (Fisher Scientific, Pittsburgh, PA), 100 units/ml of penicillin and 100 μg/ml streptomycin (Thermo Fisher, Asheville, NC), and 1 mM sodium pyruvate (Thermo Fisher, Asheville, NC). All cells were incubated at 37 °C, 10% CO_2 in a humidified environment [6, 30]. HN12 cells were nucleofected with yellow fluorescent protein (YFP) plasmids in order to portray appropriate fluorescent microscopy images and were done in the laboratory prior to this study [6].

2.2. Cytotoxicity Testing of Monolayer Cells

2.2.1. CHEMOTHERAPEUTIC TREATMENT

Both HN12 and HN6 cells were treated with each of the chemotherapeutic drugs. Cisplatin and paclitaxel (Sigma-Aldrich, St. Louis, MO) both came in powdered form, which needed to be solubilized for use. Paclitaxel was solubilized in DMSO at 50 mg/ml and then stored at -20 °C. Cisplatin was solubilized in phosphate buffered saline (PBS) at 10 mg/ml and stored at 4 °C.

Each cell line was tested with each drug. Prior to the cytotoxicity tests, cells were trypsinized and counted using an automated cell counter (Nexcelom Bioscience, Lawrence, MA). Cells were then seeded at 5×10^3 cells per well in 96 well tissue culture plates. The cells were then allowed to attach and proliferate for 24 hours in complete medium (DMEM/10% FBS). Cells were cultured in triplicate for each condition. Increasing concentrations of either paclitaxel or cisplatin were added to each cell type and were compared to the control samples, which were

cells exposed to vehicle alone (DMSO or PBS). The cells were then allowed to grow for 72 hours prior to assay.

2.2.2. WST-1 ASSAY

In order to determine the cytotoxic effects of the chemotherapeutic drugs, the WST-1 assay was used. WST-1 assay is a non-radioactive, colorimetric assay that quantifies cell viability. When compared to other cytotoxicity assays such as MTT, MTS, and XTT; WST-1 is advantageous because it is a ready-to-use reagent, no radioactive isotopes are used, there are no washing steps, and no additional reagents needed. The WST-1 assay is based on the cleavage of tetrazolium salt WST-1 to form formazan-class dyes by mitochondrial succinate-tetrazolium reductase. Therefore this process only occurs in viable cells, and is quantified by absorbance at 420-480 nm using a plate reader (BioTek Instruments, Winooski, VT). This assay is highly sensitive and has the ability to detect low cell numbers as well as being able to process a large number of samples in a multi-well format. In addition, WST-1 is water-soluble; therefore, the assay protocol is simplified because there is no need for organic solvent washing in between steps [29].

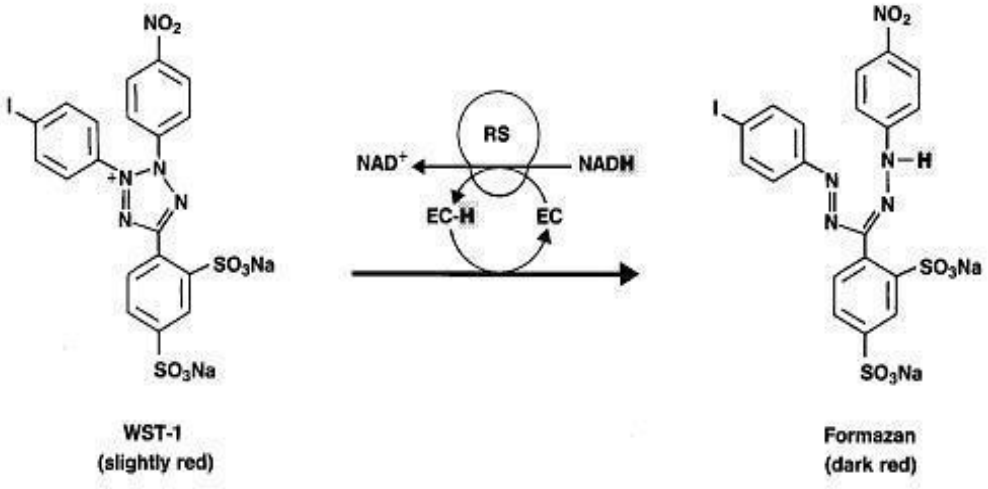

Figure 2.1: Chemical structure of tetrazolium salt cleaved to form formazan dye [29].

The IC_{90} for 2D culture of HN12 and HN6 cells in monolayer was determined by using the WST-1 assay. Cells were seeded and treated as previously described. After 72 hours of drug treatment, media/chemotherapeutic mix or control was aspirated from each well. A ten fold dilution of media to assay solution was made in order to pipette into each well seeded with cells. Thus, 90 µl media and 10 µl of assay were pipetted into each well so that 100 µl of assay mixed with media could be added to each well. The cells seeded with WST-1 and media mixture were then incubated for 40 minutes in order to allow formation of formazan dye.

2.3. Scaffold Fabrication

2.3.1. ELECTROSPINNING PARAMETERS

Electrospinning was performed in order to produce scaffolds for cell seeding as previously described. Polymer was spun onto an air impedance mandrel as seen in Figure 1.1. The air impedance mandrel was designed to allow for air to be pumped through the small holes. Air pressure is induced during electrospinning in order to generate porosity throughout the scaffold with the goal of increasing cell infiltration after seeding. For our experiments, air was not used, although the holes alone gave the possibility for increased porosity, and the same mandrel was used for consistency. The mandrel was set eleven inches away from an 18 gauge blunt needle tip in order to allow enough room to fabricate the appropriate sized jet streams and produce the precise sized fibers. A positive voltage of 25 kV was applied to the metal needle tip in congruence with an aluminum sheet grounded behind the spinning mandrel. The mandrel spun at 500 revolutions per minute while the polymer solution was pumped out of the needle at a rate of 4 ml/hr. All parameters were kept consistent for each scaffold fabricated in order to ensure consistency.

Figure 2.2: Air impedance mandrel used during electrospinning.

2.3.2. PLLA

PLLA (Sigma-Aldrich, St. Louis, MO), with a viscosity of ~2.0 dL/g, was dissolved in 1,1,1,3,3,3 Hexafluoro-2-propanol (HFP) at specific concentrations. PLLA was mixed and dissolved in HFP under the hood for a period of 24-48 hours to ensure the entire polymer was solubilized. Concentration of polymer to volume of solvent was directly correlated to the fiber diameter that was generated for each scaffold.

2.3.3. SCANNING ELECTRON MICROSCOPY

Dry scaffolds were generated by electrospinning and their morphology was evaluated by electron microscopy. Dry scaffold samples were gold sputter coated and imaged with a JEOL JSM-5610LV scanning electron microscope (SEM) in the Nanomaterials Core Characterization facility at Virginia Commonwealth University. Diameters and pore sizes were determined using NIH ImageJ (http://rsbweb.nih.gov/ij/) from 100 randomly chosen fibers and pores in each SEM image. Average fiber diameters were calculated from these 100 randomly chosen fibers from each scaffold in order to assure that the fiber sizes are consistent among each of the labeled small, medium, and large fiber diameter scaffolds [6, 30].

2.3.4. MECHANICAL TESTING

As previously described in section 1.6.3., uniaxial tensile testing was performed on each

electrospun scaffold. The three different scaffolds, containing different fiber diameters, were punch into dog-bone shaped samples (overall length of 20 mm, 2.67 mm at the narrowest point, gauge length of 7.5 mm, n=9). This type of tensile testing was performed using an MTS Bionix 200 testing system with 100 N load cell (MTS Systems, Eden Prairie, MN). Samples were pulled into tension uniaxially, along the longest axis of the samples until failure at a rate of 10mm/min (1.33/min strain rate). Calculations and readings of peak stress, modulus, energy at break, and strain at break were done through TestWorks version 4 [6].

2.3.5. PORE SIZE AND POROSITY

The pore size and porosity of the scaffolds were measured using NIH Image J (http://rsbweb.nih.gov/ij/). Three scaffolds of each fiber size were engineered and from each of these scaffolds, three samples were SEM imaged. Therefore, for each fiber size scaffold, nine total images were taken from three different scaffolds in order to ensure consistency. The SEM images were then assessed using NIH Image J by converting the images to binary and finding the edges of the fibers. Particles were analyzed with a binary, circulatory measurement of 0.01-1.00. By inputting this data, the software was able to calculate the shape of the pores. From here the pore sizes were calculated as well as the percentage of porous area (porosity).

2.3.6 STATISTICAL ANALYSIS

All quantitative data between the small fiber, medium fiber, and large fiber diameter scaffolds were compared using a one-way anlaysis of variance (ANOVA) with $p<0.05$ considered to be statistically significant. When ANOVA analysis resulted in statistically significant differences, the Tukey-Kramer test was performed to determine which data sets were significantly different. All quantitative data are presented with the standard error of the mean (s.e.m.). All statistical analysis was done using GraphPad Prism software [6].

2.4. Seeding Cells onto Fabricated Scaffolds

2.4.1. ACID PRETREATMENT

As described previously, PLLA is a very hydrophobic polymer which is less than ideal for biocompatibility. Studies have shown that acid pretreatment of scaffolds can improve the biocompatibility of hydrophobic polymers such as PLLA [33]. If scaffolds are subjected to concentrated hydrochloric acid (HCl) pretreatment the surface properties of the scaffolds are altered as well as the charge characteristics of electrospun PLLA. HCl pretreatment can be used to manipulate hydrophilic nature of the polymer and improve cellular adhesion. It has been hypothesized that improvements in hydrophilicity and adhesion are due to hydrolysis.

Therefore, scaffolds were initially disinfected in 70% ethanol for ten minutes and then rinsed three times in purified water (Millipore Corporation, Billerica, MA) under agitation for ten minutes. After water agitation, the scaffolds were then placed in 11.7 M HCl for five minutes. After immersion in HCl, it is important to make sure that the scaffolds return to a neutral pH before seeding so that the cells are able to survive in a biocompatible environment. To achieve this, the scaffolds were rinsed in PBS for ten minutes three times with agitation, until the pH is returned to a neutral state by testing with pH strips (pHydrion Papers, Micro Essential Laboratory, Brooklyn, NY). The scaffolds were then placed in media for two hours prior to seeding cells [33].

2.4.2. CELL SEEDING

Scaffold disks were punched out from a larger sheet of electrospun PLLA using 6 mm scaffold biopsy punches (Picu Punch, Ft. Lauderdale, FL). 50 μl of 70% ethanol was pipetted into each well in order to disinfect scaffolds prior to seeding. All cell types were seeded identically at a density of $1x10^4$ cells and scaffolds were anchored by 6mm diameter cloning

cylinders (Pyrex Corning Incorporated, Corning, NY). Cells were allowed to grow for 7 and 14 days and were imaged using a fluorescence microscope at both time points to ensure/confirm sufficient cell attachment and infiltration.

2.4.3. FLUORESCENCE MICROSCOPY

As mentioned above, imaging of cells on scaffolds was carried out to ensure that cells were successfully attached and had infiltrated the scaffolds. In order to do this, the cells were first fixed by placing methanol in the wells for ten minutes. The scaffolds were allowed to air dry and then placed at -80 °C. Scaffolds were permeabilized in 0.1% Triton X-100 (Shelton Scientific, Inc., Shelton, CT) in PBS at ambient temperature. 0.1% Triton X-100 is an organic solvent that, in this particular application, was used to coagulate proteins and used to fix and permeabilize cells [41]. Scaffolds were then washed with PBS three times for five minutes. Permeabilization was done in order to allow 4',6-diamidino-2-phenylindole (DAPI) to enter the cell and stain the DNA, using DAPI in PBS (1 μg/ml) for 30 minutes in the dark. After DAPI staining, the scaffolds were again washed with PBS three times for five minutes and stored in the dark until they were cryosectioned. When the scaffolds were ready to be cryosectioned, they were embedded in Neg50 frozen section medium (Thermo Fisher, Asheville, NC), cryosectioned at 10 μm and immediately mounted onto glass slides. The sectioned samples were then mounted with Vectashield Mounting Medium For Fluorescence (Vector Laboratories Inc., Burlingame, CA) and examined using a Zeiss Axiovert 200M fluorescence microscope (Carl Zeiss Microimaging, Inc, Thornwood, NY) [6].

2.4.4. LIVE/DEAD ANALYSIS

After cells had been cultured for 7 days on the small and medium fiber diameter scaffolds, they were then treated with cisplatin for 72 hours. A live/dead analysis was performed

in order to determine the survival rate of cancer cells after being treated with a chemotherapeutic drug in 3D. The scaffolds were initially washed with PBS and then were placed in the assay that correlated with either viable cells or dead cells. The scaffolds were stained with 10 µM 5-chloromethylfluorescein diacetate (CMFDA) to stain live cells and 5 µM of ethidium homodimer-1 (EthD-1) for dead cells. The disks were incubated for 40 minutes, and then washed with PBS for five minutes three times. The disks were then fixed in 4% PFA, stained with DAPI, cryosectioned, and imaged as described above. Viability was calculated by counting the percentage of live cells per field of view from five randomly chosen fields of view from three samples per condition [6].

Chapter 3

Results and Discussions

3.1. Monolayer Cell Toxicity Tests

3.1.1. PACLITAXEL TREATMENT

A monolayer of each cell line was cultured directly on 96-well culture plates. Increasing amounts were tested in triplicate from no drug to paclitaxel concentrations that elicited ~100% cell death (0% survival). After 72 hours of paclitaxel treatment, the WST-1 assay was used as a colorimetric assay to quantify cell viability. In this assay, viable cells are able to create formazan-dyes, the absorbance of which can be read in a 96-well plate reader. Absorbance was measured at 450 nm and 650 nm wavelengths, and a blank well was read simultaneously in order to subtract background noise in the absorbance calculations. Averages of the absorbances from the non-treated samples represented 100% cell viability. All other drug concentrations were compared to this in order to determine the IC_{90} concentration.

Figure 3.1 shows the percentage of HN6 cells that survive following treatment with paclitaxel. The IC_{90} calculation confirmed that 45 nM was the effective concentration needed to kill 90% of the cell population. The corresponding concentrations of paclitaxel tested on the monolayer of HN6 cells can be found in Table 3.1. These values show exact survival percentages of HN6 cells at each drug concentration and validate the IC_{90} calculation.

Table 3.1: Paclitaxel concentrations (nM) used during monolayer HN6 cell drug toxicity testing.

Paclitaxel Concentration (nM)	0	5	10	20	40	60	100
HN6 Cell Survival (%)	100	45	33	23	13	6	4

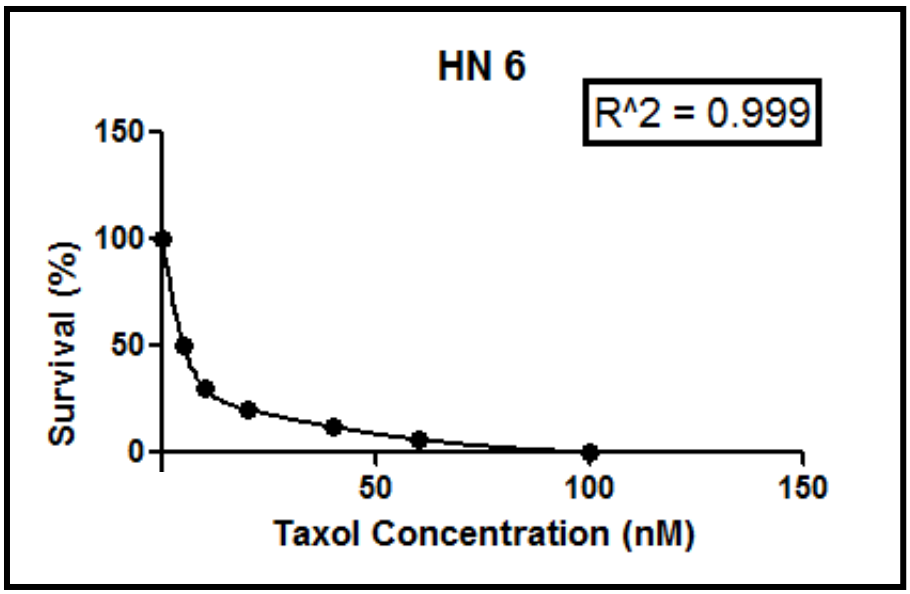

Figure 3.1: HN6 cells are sensitive to paclitaxel in 2D culture. HN6 cells were grown in 2D culture, then incubated with the indicated doses of paclitaxel for 72 hours. A formazan dye viability assay was performed to construct the dose response curve and 45nM paclitaxel was determined to be the IC_{90} (n=15).

HN12 cell culture and paclitaxel treatment were identical to the drug toxicity tests performed on HN6 cells. To keep a consistent comparison between the two cell lines, the same concentrations for paclitaxel were tested on the monolayer of HN12 cells. The IC_{90} calculations from these tests indicated that 98 nM paclitaxel was needed to kill 90% of the cell population (Figure 3.2). Table 3.2 displays the concentrations used during drug testing and the corresponding cell survival percentages.

Table 3.2: Paclitaxel concentrations (nM) used during monolayer HN12 cell drug toxicity testing.

Paclitaxel Concentration (nM)	0	5	10	20	40	60	100
HN12 Cell Survival (%)	100	43	35	28	20	17	8

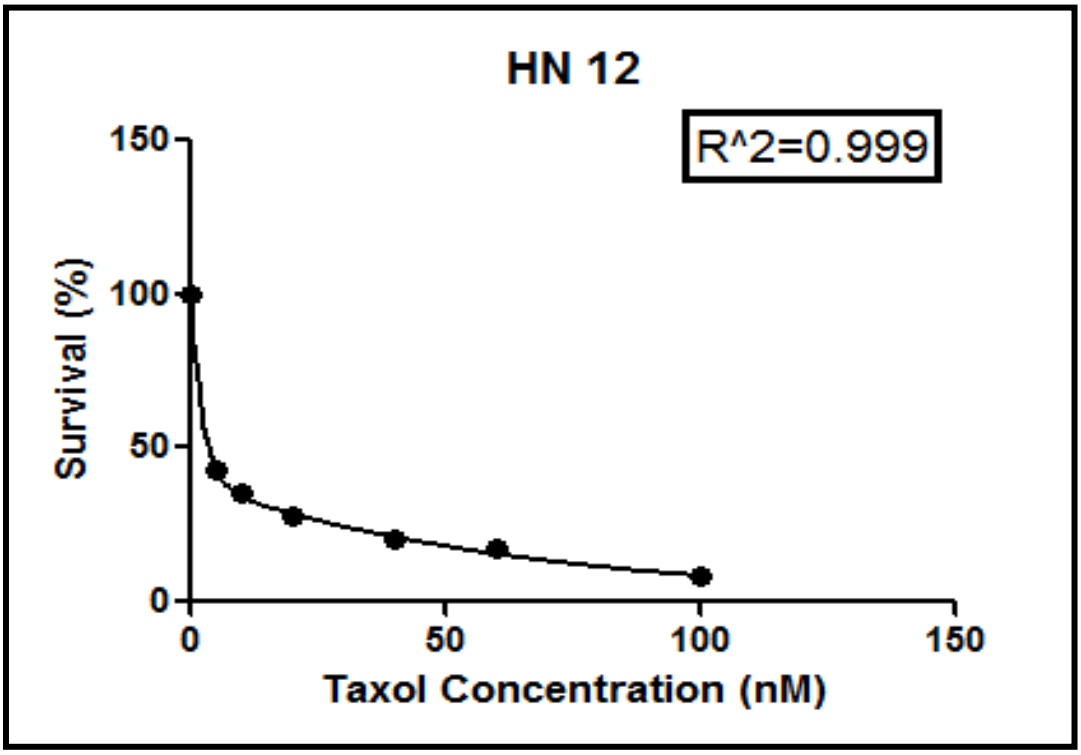

Figure 3.2: HN12 cells are sensitive to paclitaxel in 2D culture. HN12 cells were grown in 2D culture, then incubated with the indicated doses of paclitaxel for 72 hours. A formazan dye viability assay was performed to construct the dose response curve and 98nM Taxol was determined to be the IC_{90} (n=15).

3.1.2. CISPLATIN TREATMENT

HN12 and HN6 cells were cultured as monolayers as previously described, and were then treated with increasing amounts of cisplatin for 72 hours. All absorbance readings from the WST-1 assay were analyzed as outlined above, resulting in decreasing cell survival with increasing concentrations of cisplatin.

HN 6 monolayer cells were found to be very sensitive to cisplatin. Cisplatin was potent at low concentrations, and as the drug concentration increased, 100% of cells were killed (Figure 3.3). The calculated IC_{90} for cisplatin in HN6 monolayer drug testing was 6µg/ml. Increasing concentrations resulted in 0% of the HN6 cells remaining viable (Table 3.3).

Table 3.3: Cisplatin concentrations (µg/ml) used during monolayer HN6 cell drug toxicity testing.

Cisplatin Concentration (µg/ml)	0	2.5	4	5	6	8	10	20	40	50
HN6 Cell Survival (%)	100	53	39	18	11	4	2	0	2	0

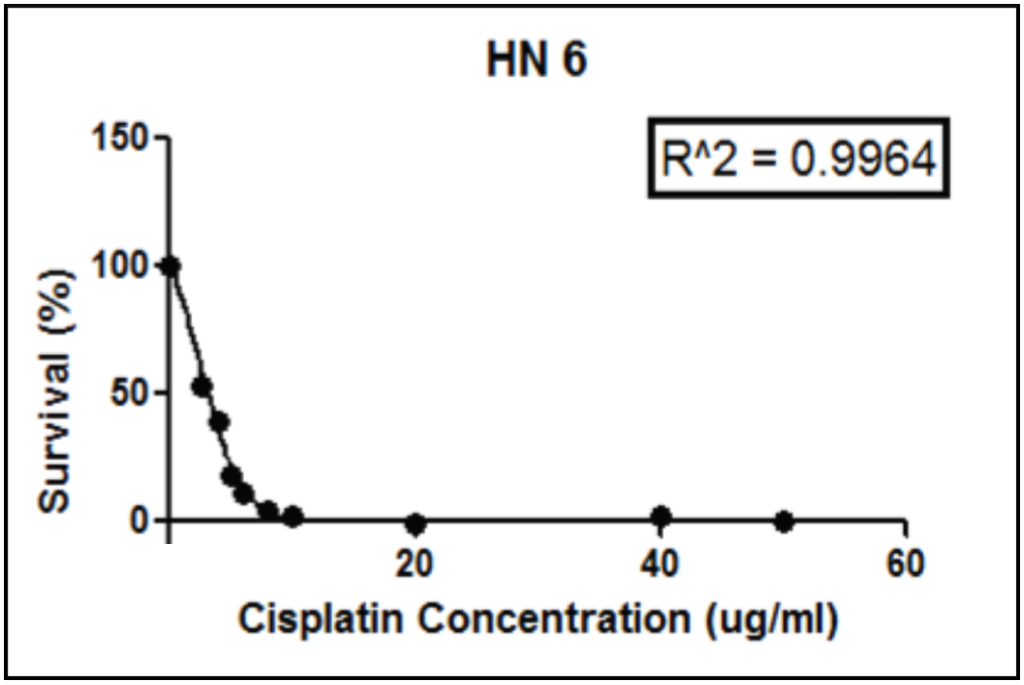

Figure 3.3: HN6 cells are sensitive to cisplatin in 2D culture. HN6 cells were grown in 2D culture, then incubated with the indicated doses of cisplatin for 72 hours. A formazan dye viability assay was performed to construct the dose response curve and 6 µg/ml cisplatin was determined to be the IC_{90} (n=21).

HN12 cells were treated identically to HN6 cells with the same concentrations of cisplatin. The data remained consistent with those for HN6 cells cultured in monolayers in that HN12 cells were sensitive to cisplatin (Figure 3.4). An IC_{90} of 5µg/ml was determined for HN12 cells in monolayer, which was close to the IC_{90} value of HN6 treated with cisplatin. Table 3.4 shows HN12 cell survival with each cisplatin drug concentration.

Table 3.4: Cisplatin concentrations (µg/ml) used during monolayer HN12 cell drug toxicity testing.

Cisplatin Concentration (µg/ml)	0	2.5	4	5	6	8	10	20	40	50
HN12 Cell Survival (%)	100	65	22	18	1	0	0	0	2	0

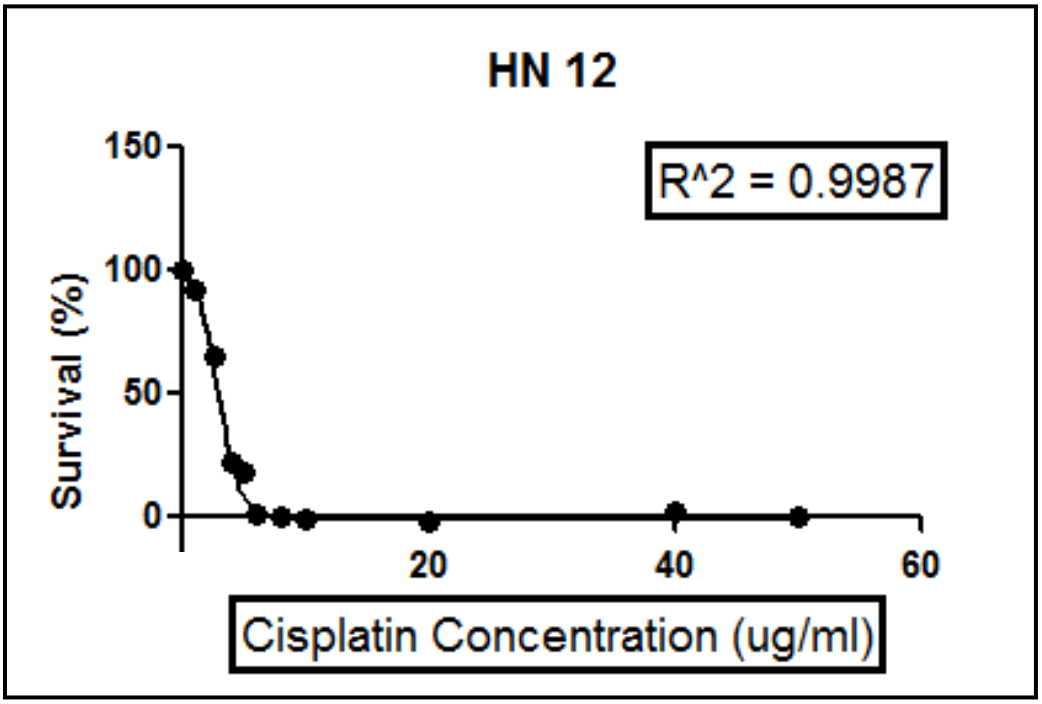

Figure 3.4: HN12 cells are sensitive to cisplatin in 2D culture. HN12 cells were grown in 2D culture, then incubated with the indicated doses of cisplatin for 72 hours. A formazan dye viability assay was performed to construct the dose response curve and 5 µg/ml cisplatin was determined to be the IC_{90} (n=36).

3.1.3. IC_{90} CALCULATIONS AND RESULTS

A statistical tool (GraphPad Prism) was used in order to calculate the IC_{90} value for each cell type and its corresponding drug treatment. Absorbance data, including averages of all survival percentages, standard deviations, and number of samples were extracted from Microsoft Excel and translated to GraphPad Prism where a drug dose response analysis was performed. The software was able to compute values needed for IC_{90} calculations such as IC_{50} and Hill slope (H). These values were then used in IC_{90} calculation (Equation 1) [39].

$$IC_{90} = IC_{50} + \left(\left(\frac{1}{H}\right) * log_{10}(9)\right) \quad \text{Equation 1}$$

Table 3.5: Overview of calculated IC_{90} for both HN6 and HN12 treated with either paclitaxel or cisplatin.

	HN6	HN12
Paclitaxel (nM)	45	98
Cisplatin (µg/ml)	6	5

3.2. Monolayer Cell Toxicity Tests: Conclusions

It was found that both cell types, HN6 and HN12, were sensitive to both paclitaxel and cisplatin. Compared to previous *in vitro* doses of 40nM, there was less sensitivity to paclitaxel [6]. While comparing the differences in drug dose responses between HN6 and HN12 cells in monolayers, HN6 cells were found to be more sensitive to paclitaxel. Therefore, a lower concentration of paclitaxel was needed to kill HN6 cells than HN12 cells. HN12 cells may be more resistant to paclitaxel because of their higher doubling time compared to HN6. Although, exact doubling times were not calculated in these experiments, HN12 cells in 2D culture were shown to proliferate at a faster rate than HN6 cells. Paclitaxel works by targeting the cell cycle and arresting the cells in mitosis. It could be possible that at the time of treatment not all of the HN12 cells were in the M stage of the cell cycle due to its rapid cell cycle. It has been found that cell death is markedly reduced in cells blocked at the G_1-S transition phase [40].

As discussed earlier, both HN6 and HN12 were notably sensitive to similar small dosages of cisplatin. Cisplatin has an anti-tumor effect by directly binding to DNA, causing platinum DNA monoadducts. These adducts can then inhibit cell proliferation, and if the DNA is not repaired, cell death can occur [43]. Since cisplatin does not target a stage of the cell cycle, but rather a vital structure of the cancer cells, this could explain the high sensitivity experienced by both HN6 and HN12 cells. There is also a possibility that HN6 and HN12 have a higher level of microtubule resistant mechanisms, which would reduce the effects of mitotic arrest caused by paclitaxel. These cell lines might also have a lower level of platinum to DNA binding resistant mechanisms which would enhance the effects of cisplatin. Clinical doses of cisplatin effectively and consistently killed both HN6 and HN12 monolayer cell lines, therefore it was decided that a concentration of 6 μg/ml of cisplatin would be used for future drug testing in 3D models.

3.3. Scaffold Fabrication

3.3.1. QUANTIFYING SMALL, MEDIUM, AND LARGE FIBER DIAMETER SCAFFOLDS

Differences in fiber dimensions were investigated in order to understand how fiber diameter affects the growth of cells and drug efficacy in a 3D *in vitro* cancer model. As explained previously, engineered scaffolds represent the microenvironment of a tissue. Scaffolds are engineered ECM designed to support host cells and elicit an environment where host cells can regenerate tissue. Tissue engineering provides the possibility to manipulate several different parameters within the engineered ECM. Altering parameters in the engineered scaffold will result in different cellular functions.

In this study, the ECM parameter of interest to investigate was fiber diameter size: small, medium, and large, which were directly related to nanofiber sizes produced during electrospinning of PLLA. The concentration of PLLA polymer solution in HFP was directly related to the size of fibers produced. It was found that 55 mg/ml was the lowest polymer concentration that electrospun the smallest fiber diameters without causing any beading of the polymer. It is often found that electrospun fibers will have beads as "by products" which is related to the instability of the jet polymer, or that the polymer concentration is too low [41]. The polymer concentration of PLLA required to produce the largest size fibers was 180 mg/ml. A concentration of 115 mg/ml produced fibers of medium diameter, which was a midpoint between the small and large concentrations. These three fiber sized scaffolds were quantified and characterized prior to introducing any cell lines.

In order to quantify the three different fiber sizes, the scaffolds were imaged by SEM and the fiber diameters were measured with NIH ImageJ. Three scaffolds were made for each fiber

size, and three samples were taken from each scaffold. Therefore, nine randomly selected images of each scaffold size were produced. 100 fiber width measurements in total were made for each scaffold size using the length-measuring tool in NIH ImageJ. Figure 3.5 shows comparative SEM images of the three different fiber diameters. A linear relationship between PLLA concentration and fiber diameter is represented in Figure 3.6. It was found that for small, medium, and large the average fiber widths were 0.5 µm, 1.7µm, and 5.1 µm respectively.

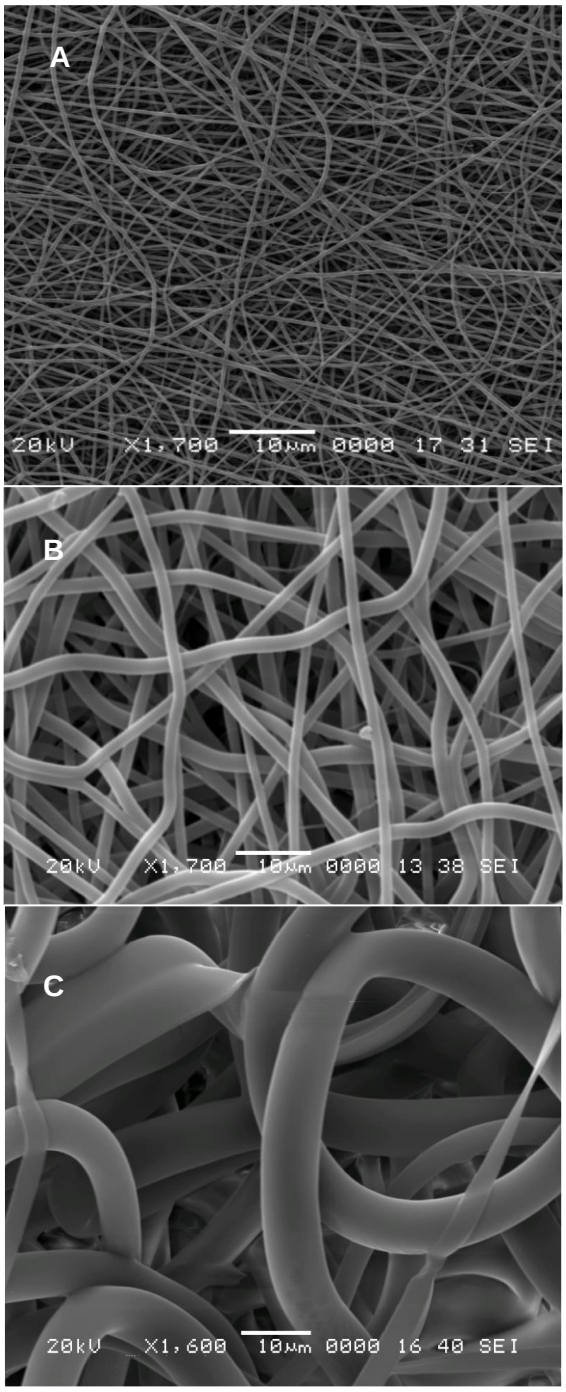

Figure 3.5: SEM image of (A) small fiber diameters, (B) medium fiber diameters, and (C) large fiber diameters constructed by electrospinning polymer solution of 55mg/ml, 115mg/ml, and 180mg/ml of PLLA into HFP respectively. The average fiber diameter width was 0.5±0.2µm, 1.7±0.3µm, and 5.1±1.2µm for small, medium, and large respectively (n=100).

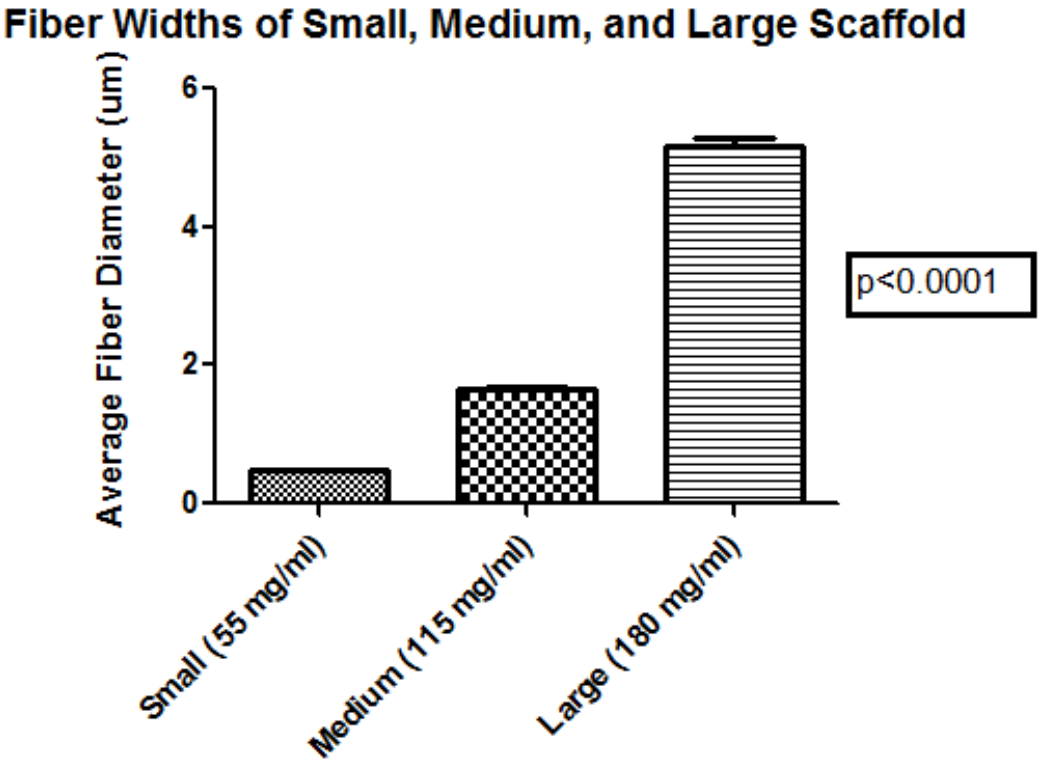

Figure 3.6: Graphical comparison of average fiber diameters between small, medium, and large fiber diameter scaffolds. Measurements were made using ImageJ (n=100, +/-s.e.m.).

3.3.2. UNIAXIAL TENSILE TESTING

Collecting mechanical data is a helpful tool to compare different tissue engineered scaffolds. There are several reasons why it is imperative to test scaffolds under mechanical stresses, for example the scaffold material may need to undergo harsh stresses and strains in an artificial artery. For this study, mechanical testing was used in order to compare the properties of small, medium, and large fibers. The goal was to explore ideal mechanical properties needed for cell seeding and infiltration in cancer models.

Uniaxial tensile testing was done using an MTS Bionix testing system with a 100 N load cell, as described previously. For each of the fiber sized scaffolds, width, thickness, peak load, peak stress, modulus, strain at break, and energy at break were calculated using TestWorks version 4. Table 3.6, Table 3.7, and Table 3.8 show the mechanical data for small, medium, and large fiber scaffolds, respectively. Three scaffolds were electrospun for each concentration and three dog bone shapes were punched out of each scaffold. Therefore, nine total tensile tests were made for each fiber size scaffold. Graphical comparisons of different mechanical parameters between the small, medium, and large fiber scaffolds can be seen in Figure 3.7.

Table 3.6: Unaxial tensile testing of PLLA for small fiber diameter scaffolds. (n=9).

Small							
	Width (in.)	**Thickness (in.)**	**Peak Load (N)**	**Peak Stress (Mpa)**	**Modulus (Mpa)**	**Strain at Break (mm/mm)**	**Energy To Break (N*mm)**
Mean	0.105	0.00256	0.631	5.55	59.4	0.265	0.849
S.D.	1.46E-17	0.00172	0.251	3.36	35.7	0.0581	0.41

Table 3.7: Unaxial tensile testing of PLLA for medium fiber diameter scaffolds. (n=9).

Medium							
	Width (in.)	**Thickness (in.)**	**Peak Load (N)**	**Peak Stress (Mpa)**	**Modulus (Mpa)**	**Strain at Break (mm/mm)**	**Energy To Break (N*mm)**
Mean	0.105	0.00711	1.62	3.36	96.2	0.188	1.84
S.D.	1.46E-17	0.00129	0.515	0.735	28.2	0.0418	0.864

Table 3.8: Unaxial tensile testing of PLLA for large fiber diameter scaffolds. (n=9).

Large							
	Width (in.)	**Thickness (in.)**	**Peak Load (N)**	**Peak Stress (Mpa)**	**Modulus (Mpa)**	**Strain at Break (mm/mm)**	**Energy To Break (N*mm)**
Mean	0.105	0.0165	1.75	1.57	2.11	2.78	1.52
S.D.	1.46E-17	0.317	0.317	0.284	0.554	0.345	0.375

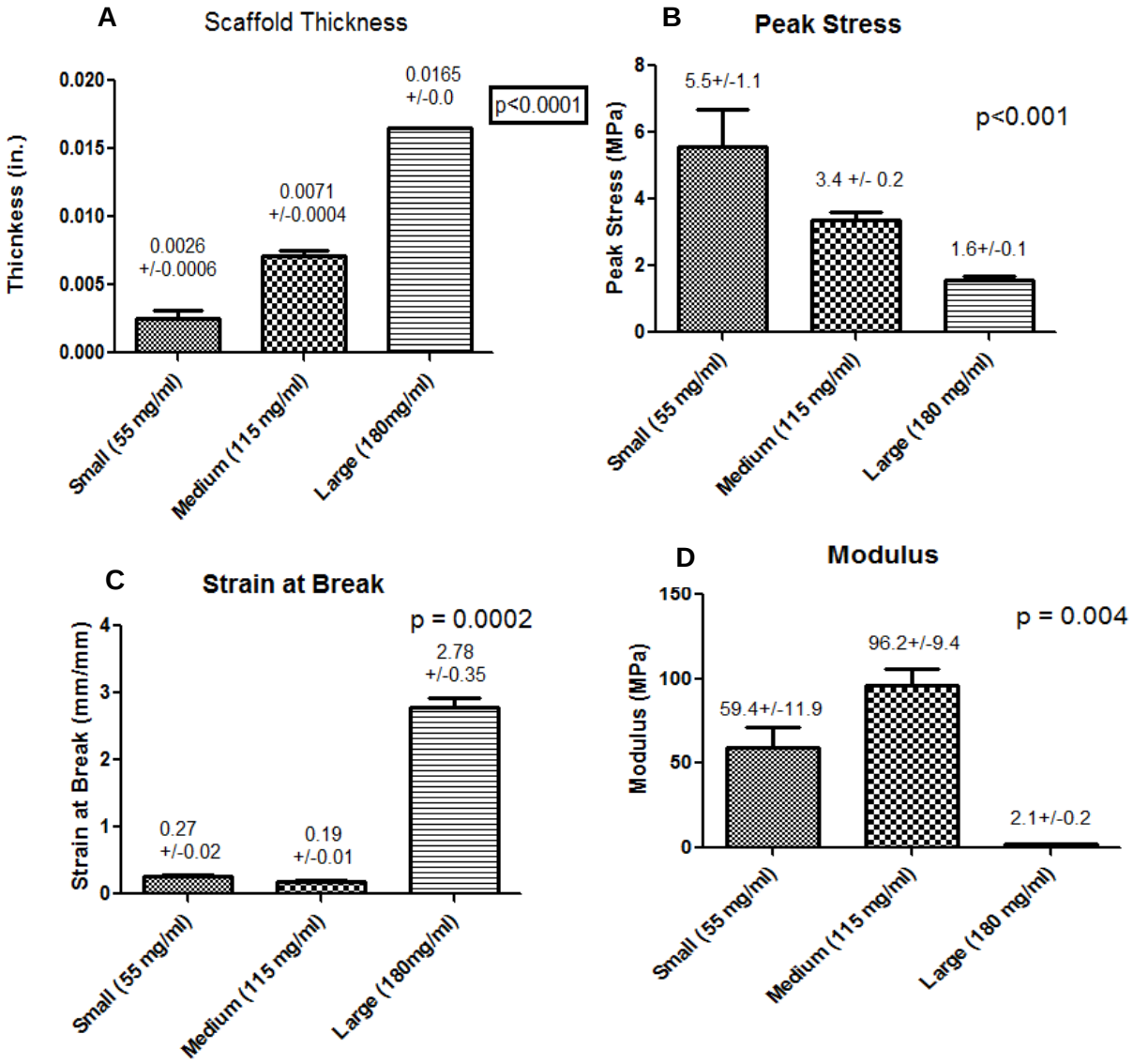

Figure 3.7: Graphical comparison of (A) average thickness, (B) peak stress, (C) strain at break, and (D) modulus between small, medium, and large fiber diameter scaffolds. Measurements were made with hand-held calipers and MTS machine (n=9).

3.3.3. ANALYSIS OF SCAFFOLD PORE SIZES AND POROSITY

Porosity and pore size of 3D scaffolds have direct implications for the functionality of the scaffold during biomedical applications. It is essential to have a porous ECM so there are interconnected networks of cell nutrition, proliferation, and migration for tissue vascularization. High porosity enables the release of bio factors including genes, proteins, cells, and nutrient exchange. A porous scaffold also serves to maintain structural stability of the biomaterial through its interconnected networking of fibers [42].

SEM Images of the small, medium, and large fiber size scaffolds were assessed using NIH ImageJ. The software was able to transfer the images to black and white, find the edges, and calculate the amount of area that represented pores as well as the average pore size. Three scaffolds were electrospun for each fiber size, and three samples were imaged through SEM. Nine total images for each fiber size were evaluated for average pore size and porosity. The average pore sizes for small, medium, and large fiber scaffolds were 2.8±0.7 μm^2, 6.6±1.2 μm^2, and 5.7±2.0 μm^2 respectively (Figure 3.8 A). As fiber size increased, there was a relative increase in pore size with variability in some of the large fiber scaffolds. Porosity decreased with the increase in fiber diameter. The porosities of the small, medium, and large fiber scaffolds were 53.8±3.3 %, 42.5±1.9 %, and 26.0±2.5 % respectively (Figure 3.8 B).

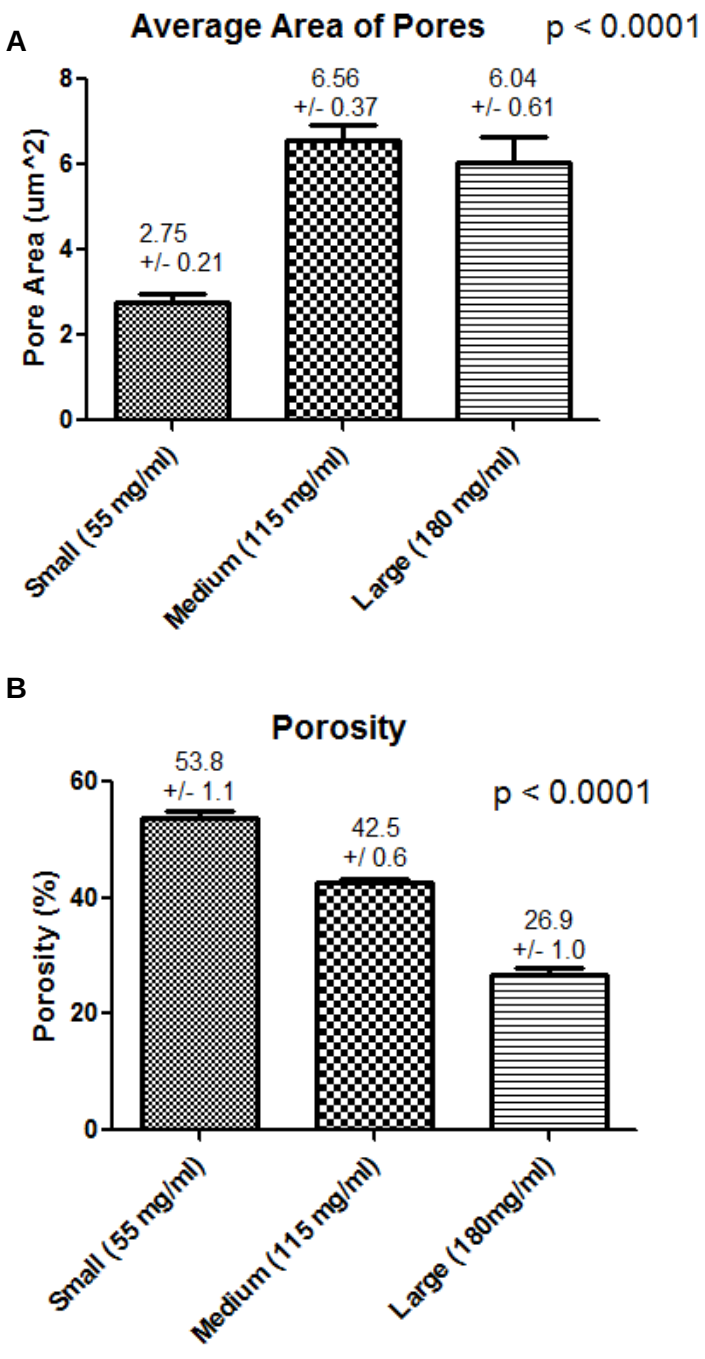

Figure 3.8: Graphical comparison of (A) average area of pores and (B) porosity between small, medium, and large fiber diameter scaffolds. Measurements were made using ImageJ. (n=9,+/- s.e.m.).

3.4. Scaffold Fabrication: Conclusions

Several parameters were examined during scaffold fabrication; the primary design parameter that was desired for comparison was different fiber widths. The goal was to design three different scaffolds comprised of all small fibers, all medium fibers, or all large fibers. These fiber dimensions were generated by electrospinning different concentrations of PLLA polymer. It was found that there was a linear relationship between PLLA concentration and fiber diameter (Figure 3.6). Optimal concentrations of PLLA were found to be 55 mg/ml, 115 mg/ml and 180 mg/ml for generating small, medium, and large diameter fibers, respectively. In order to define these concentrations it was important to determine when the fibers were too unstable, or the concentration was too low, *versus* when the polymer was unable to electrospin because the concentration was too high. Parameters were manipulated to design the small and large fiber sizes. A concentration in the middle range of these two concentrations was then chosen to generate medium size fibers.

Uniaxial tensile testing was performed on each of the scaffold types in order to compare mechanical properties between the three fiber sizes. There was a positive correlation between increase in fiber diameter and thickness of the scaffolds. It was apparent that the small fiber scaffolds were the weakest material considering they were the thinnest and they required the least amount of energy to break. The medium fiber scaffolds were the most elastic material as seen by the large modulus and small strain experienced at break. Both small and medium size fiber scaffolds could be defined as brittle structures based on their mechanical data. The large scaffolds showed the highest plastic deformation with a large strain at break value and a small modulus. The large fiber scaffolds took a great amount of energy to break because of the thickness and high ductility (Tables 3.6, 3.7, 3.8).

Pore size and porosity are two vital parameters to consider while characterizing tissue engineered scaffolds. In this study, it was desired to have cancer cells infiltrate throughout the cancer model to most accurately represent a 3D *in vivo* tumor. With ideal porosity, cells are able to freely move throughout the scaffold. With interconnected networks the cancer cells would be able to diffuse the necessary bio factors (cells or nutrient exchange) to regenerate an appropriate tumor model. It has also been found that porous scaffolds serve to maintain the structural stability of the biomaterial [42]. The data show that pore size increased as the fiber diameter increased. Therefore, the small fibers had the smallest pore sizes whereas the medium and large fibers had larger pore sizes (Figure 3.8 A). Larger pore sizes, as well as large fibers, allow for a stronger interconnected network therefore explaining why the medium fibers yielded a higher modulus and the large fibers took the most energy to break.

It is also important to note that there was a negative correlation between fiber size and porosity (Figure 3.8 B). Although the pore sizes did in fact increase with larger fibers, the overall percentage of pores per scaffold area decreased. Higher porosity suggests that smaller and medium fiber size scaffolds, average diameters of 500 nm and 1.7 μm respectively, could elicit better cell infiltration. Literature reporting similar nano-scale fiber diameters has concluded in successful cell infiltration, although with use of different cells and different electropsun polymers [46, 47]. It also could be possible that the thickness of the scaffolds affects cell infiltration: the thinner the scaffold, the easier it is for cells to travel through. When compared to previous reports in the literature, it appears that the scaffolds were around 20μm thick which was significantly thinner than each of the scaffolds imaged in this study [46].

3.5 Analysis of Cell Infiltration in Fabricated Scaffolds

In order to design an appropriate *in vitro* cancer model for testing chemotherapeutic drugs, it was essential to ensure that cells are able to seed throughout the scaffold. The 3D model was designed with the intention of testing chemotherapeutic drugs in an environment that more closely represented conditions *in vivo*. Therefore, it was critical to assess whether or not the cells were infiltrating throughout the scaffold. Cancer cells penetrating the entirety of the scaffold would more accurately represent the microenvironment of a 3D tumor.

After fabrication, scaffolds were seeded with either HN6 or HN12 cells as described previously. Comparisons were made between cell types, fiber diameters, and length of time in cell culture. Medium and small fiber diameter scaffolds were used to seed cells on and were imaged after either seven days or fourteen days to conclude whether or not time was a crucial factor. Images, using fluorescent microscopy, show the scaffolds and cells in phase, stained with DAPI, and a merged image of phase with DAPI stained cells. From these fluorescent images, cell infiltration could be examined based on the different parameters. Experiments for cell migration were run in triplicate for each condition, fiber size and culture time.

HN6 cell infiltration of small fiber diameter scaffolds can be seen in Figure 3.9. The average thickness of the scaffold shown here was 49.0 +/- 2.8 μm (n=10). Figure 3.10 shows the size difference in medium sized fibers, where the average thickness of the scaffold was 83.1 +/- 4.2 μm (n=10). HN12 cell infiltration can be seen in Figures 3.11 and 3.12 after day seven and day fourteen, respectively, of cell seeding. The small fiber scaffold in Figure 3.11 showed an average thickness of 44.5 +/- 5.5 μm (n=10), whereas the medium fiber scaffold in Figure 3.12 had an average thickness of 166.8 +/- 23.4 μm (n=10). Figure 3.13 shows the results from HN6 cells seeded on to small fibers after fourteen days with the average scaffold thickness being

54.5 +/- 5.0 μm (n=10). Figure 3.14 shows in contrast HN6 cells seeded for fourteen days onto medium fiber sizes with a scaffold thickness of 119.6 +/- 9.2 μm (n=10). HN12 cells were done identically to HN6 experiments and Figures 3.15 and 3.16 show HN12 cellular infiltration on small fibers and medium fibers respectively. Average thicknesses of small and medium scaffolds were 58.0 +/- 4.2 μm (n=10) and 119.6 +/- 9.2 μm (n=10) respectively. It is noted that for Figures 3.15 and 3.16, HN12 cells were labeled with YFP; therefore four channels were used during fluorescent microscopy.

3.5.1. DAY 7 CELLULAR INFILTRATION

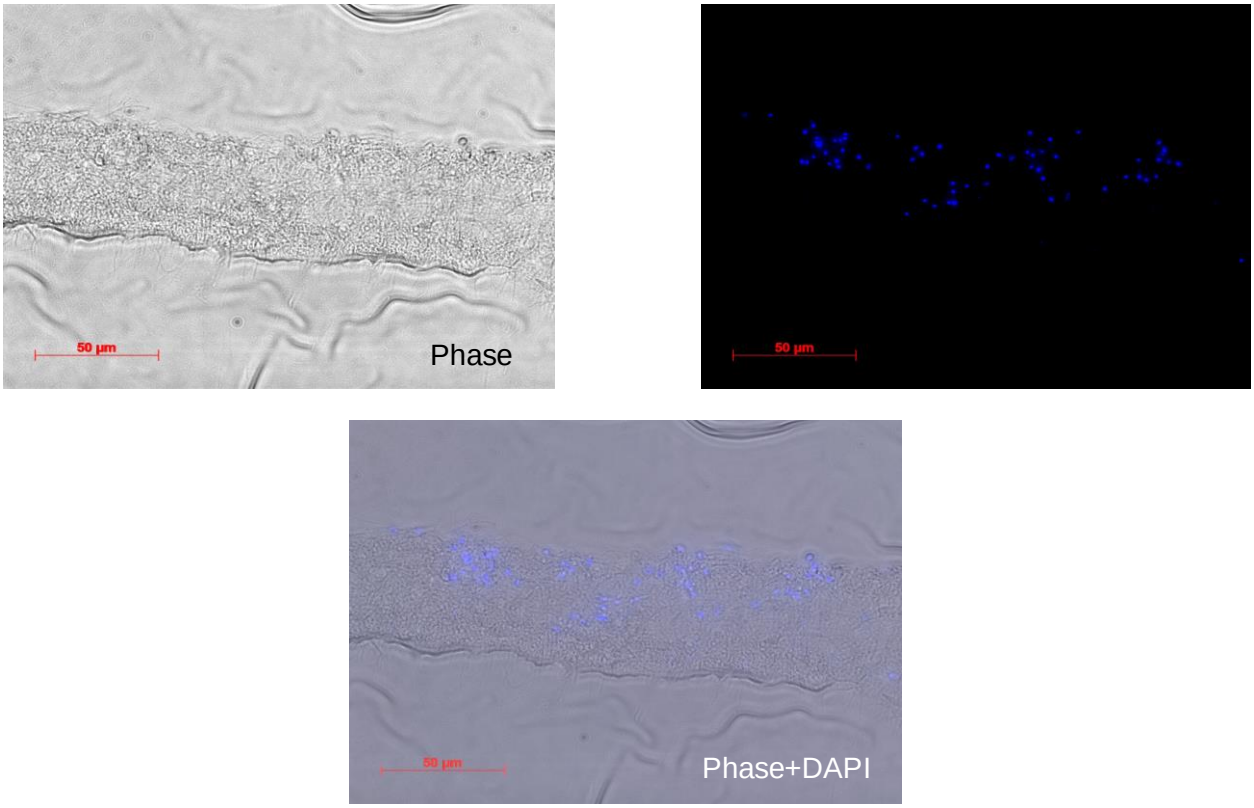

Figure 3.9: Day 7 HN6 cellular infiltration of small fiber scaffolds. The average thickness of this scaffold is 49.0 +/- 2.8 µm (n=10).

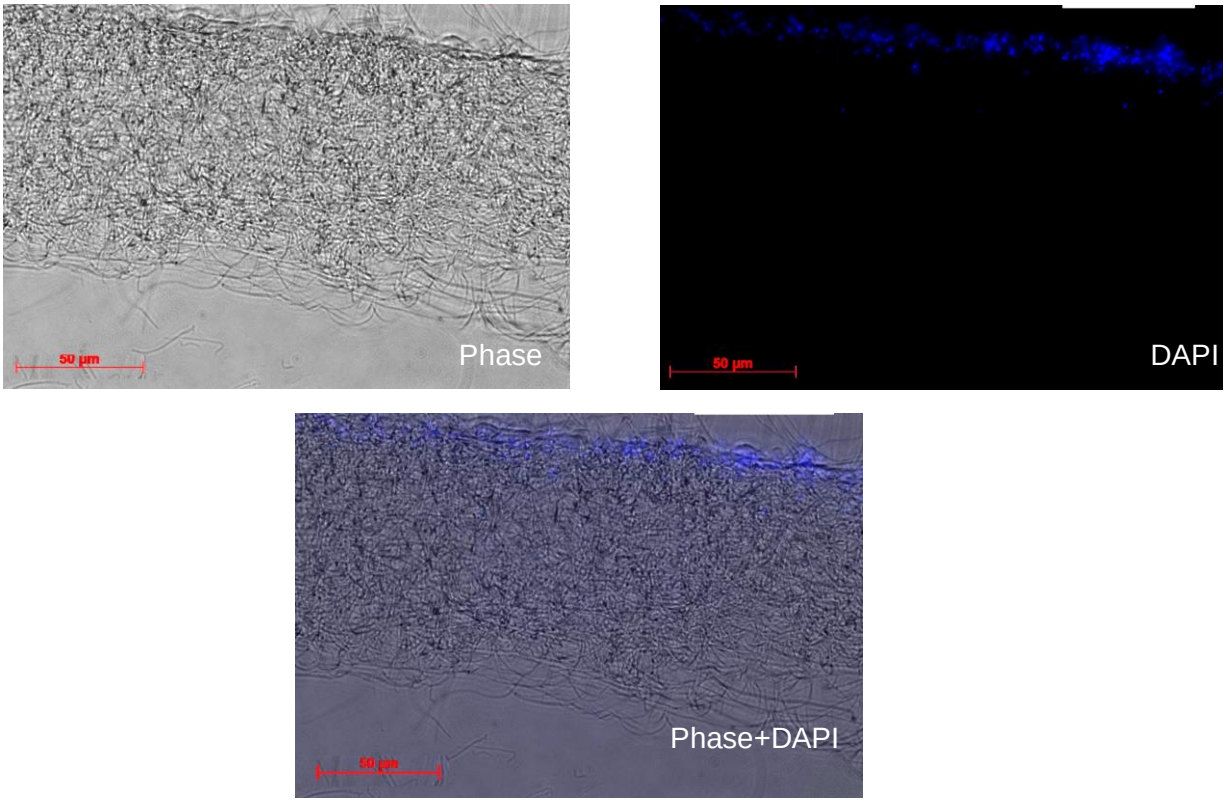

Figure 3.10: Day 7 HN6 cellular infiltration of medium fiber scaffolds. The average thickness of this scaffold is 83.1 +/- 4.2 µm (n=10).

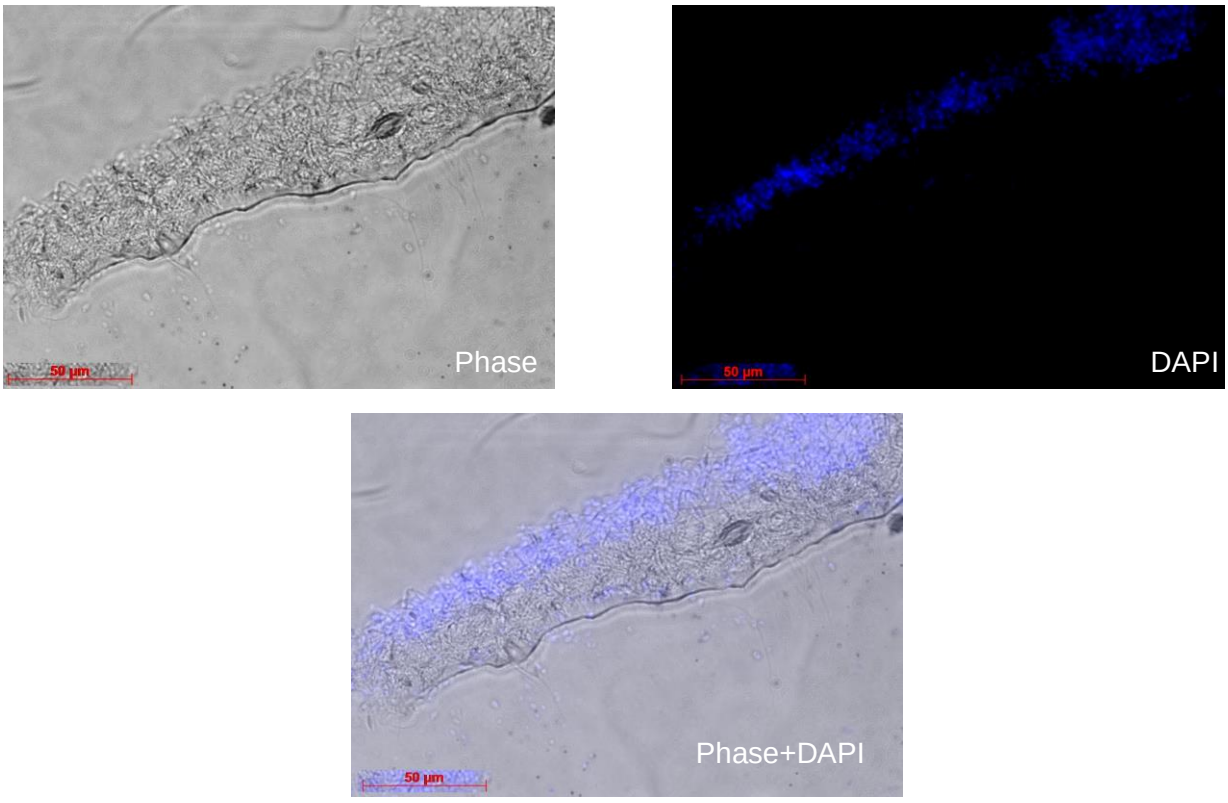

Figure 3.11: Day 7 HN12 cellular infiltration of small fiber scaffolds. The average thickness of this scaffold is 44.5 +/- 5.5 µm (n=10).

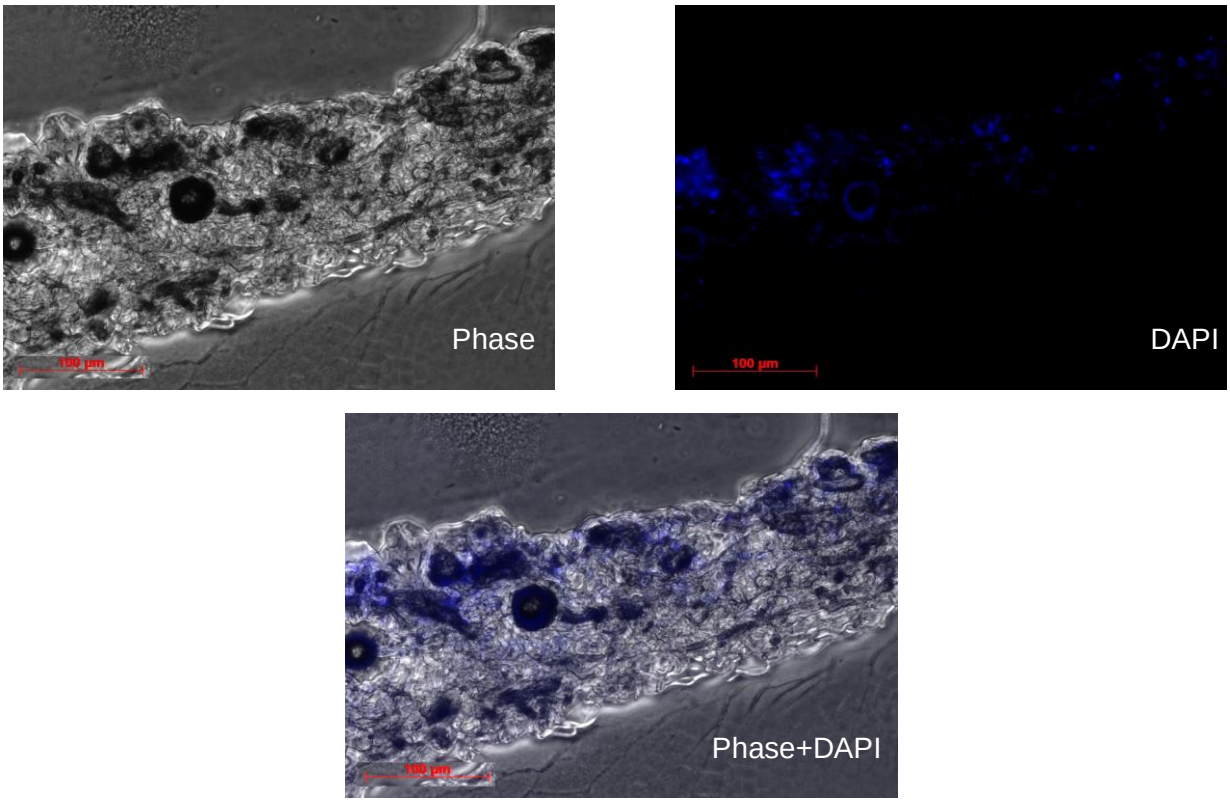

Figure 3.12: Day 7 HN12 cellular infiltration of medium fiber scaffolds. The average thickness of this scaffold is 166.8 +/- 23.4 µm (n=10).

3.5.2. DAY 14 CELLULAR INFILTRATION

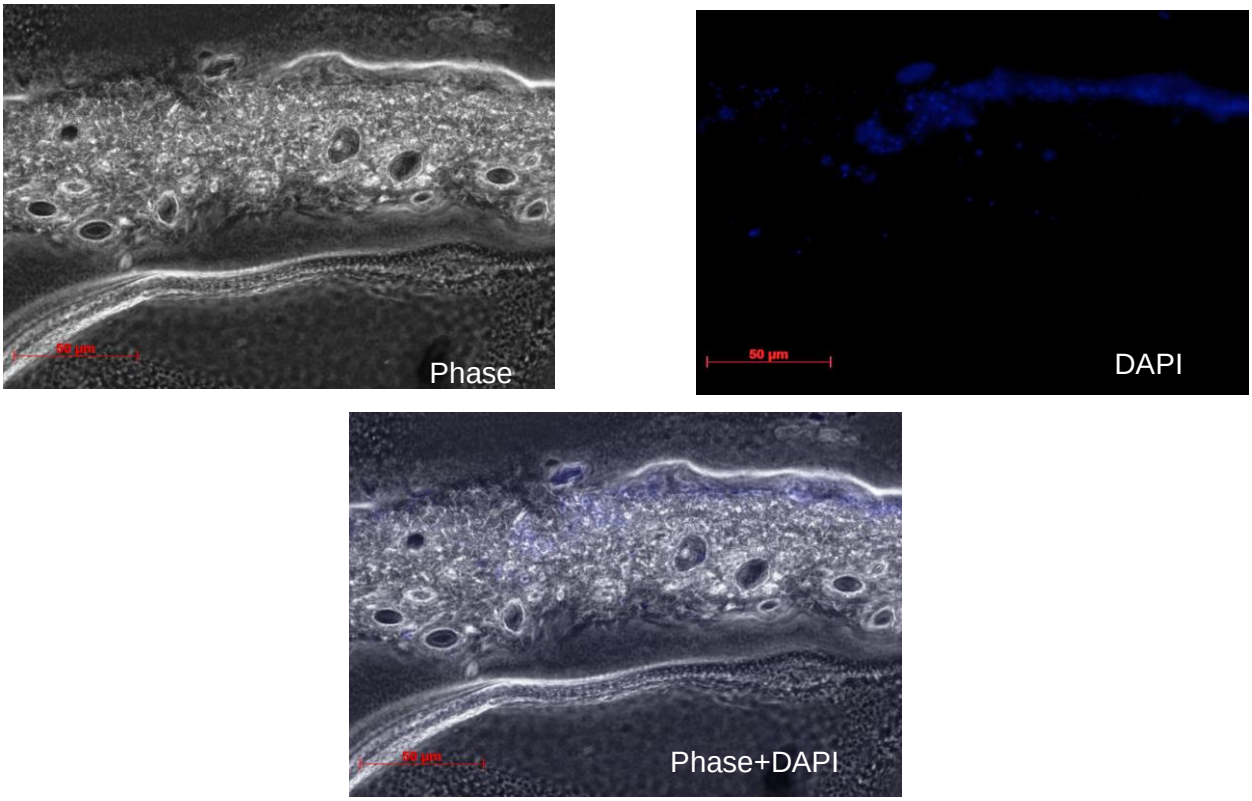

Figure 3.13: Day 14 HN6 cellular infiltration of small fiber scaffolds. The average thickness of this scaffold is 54.5 +/- 5.0 µm (n=10).

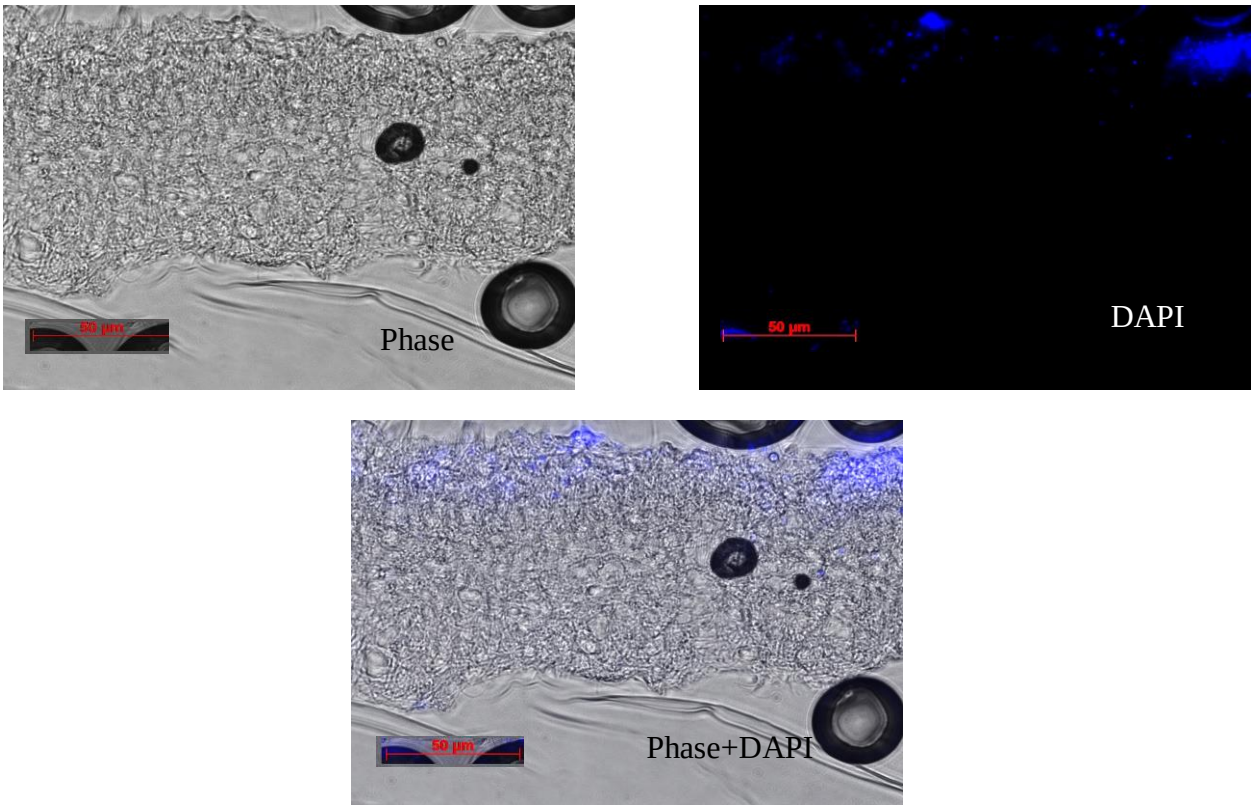

Figure 3.14: Day 14 HN6 cellular infiltration of medium fiber scaffolds. The average thickness of this scaffold is 119.6 +/- 9.2 µm (n=10).

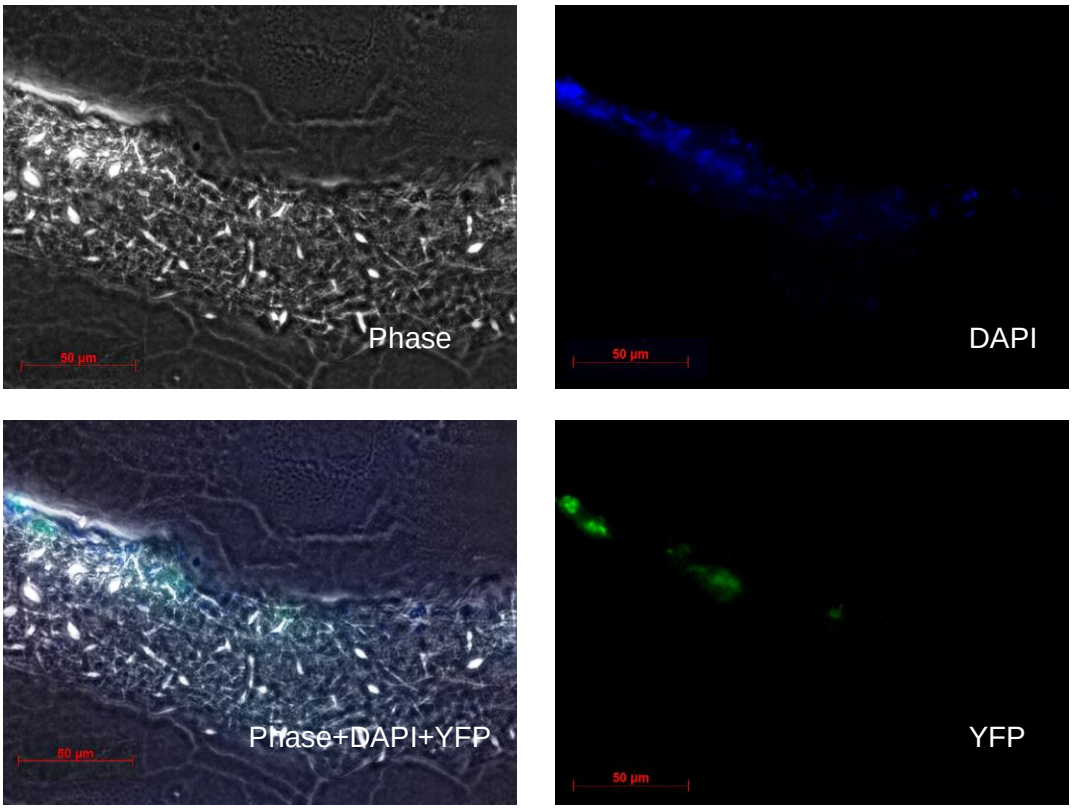

Figure 3.15: Day 14 HN12/YFP cellular infiltration of small fiber scaffolds. The average thickness of this scaffold is 58.0 +/- 4.2 µm (n=10).

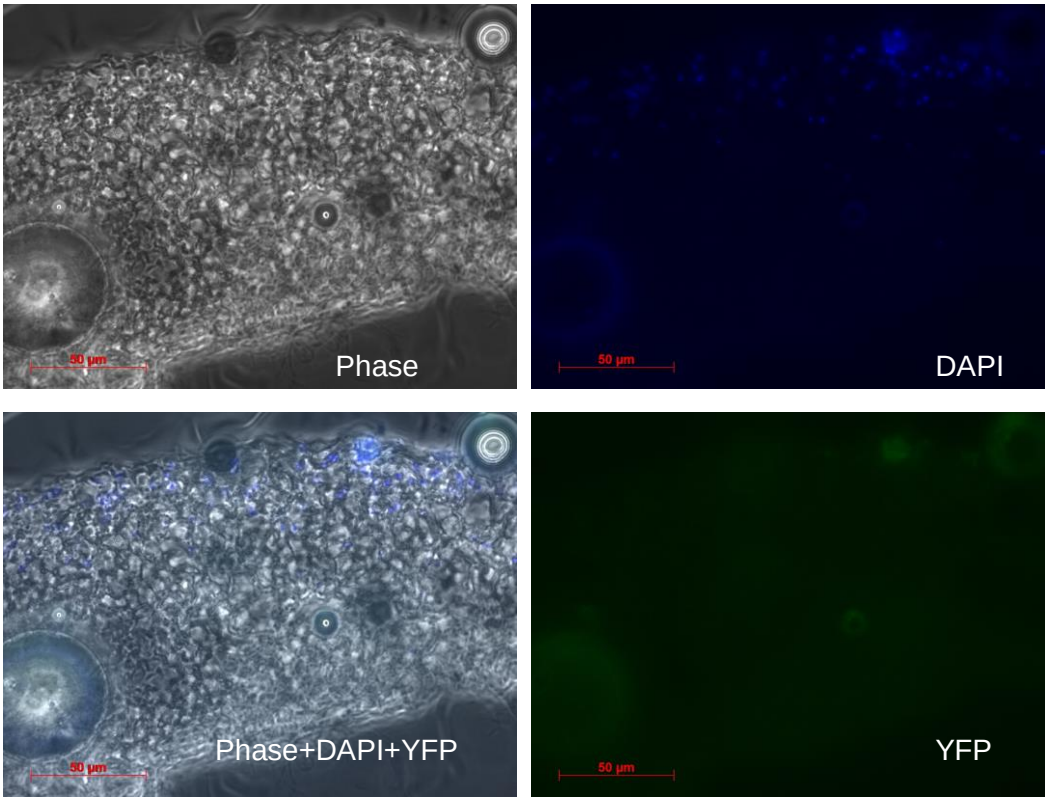

Figure 3.16: Day 14 HN12/YFP cellular infiltration of medium fiber scaffolds. The average thickness of this scaffold is 119.6 +/- 9.2 µm (n=10).

3.6. Analysis of Cell Infiltration in Fabricated Scaffolds: Conclusions

HN6 and HN12 cells were seeded onto small and medium fiber size scaffolds for periods of seven days and fourteen days in order to analyze cell infiltration. It was decided to eliminate using large fiber scaffolds because the thicker material prevented cryosectioning. Because of the inability to cryosection, large fiber scaffolds were being shredded and inaccurate representations of cell infiltration were being imaged. Therefore, cell seeding was only implemented on small and medium fiber scaffolds.

HN6 cells, after seven days of culturing on small fiber scaffolds (Figure 3.9), showed significant infiltration. The HN6 cells infiltrated throughout the majority of the thickness of the scaffold, 49.0+/- 2.8 µm, which could be due to a higher percentage of porosity throughout the scaffold. In contrast, HN6 cells seeded on the medium fiber scaffolds for seven days appeared to maintain a monolayer on the surface of the scaffold (Figure 3.10). The medium fiber scaffolds were about double the thickness (83.1 +/- 4.2 µm) of the small fiber scaffolds which could inhibit cell infiltration. As seen in Figure 3.10, the fibers are a larger size than in the smaller fiber scaffolds which results in larger pores. However, this also constitutes for a smaller porosity throughout because of the larger area of fibers, which may result in a lack of cell infiltration.

Figure 3.11 shows HN12 cells cultured for seven days on small fiber scaffolds of comparable thickness (44.5 +/- 5.5 µm) to scaffolds used for HN6 cell seeding. A large portion of the scaffold appears to be infiltrated by HN12 cells, although not as noticeable as with HN6 cells. In comparison to medium size fiber scaffolds seeded with HN12 cells for seven days, the scaffold was approximately four times thicker than the small scaffold (166.8 +/- 23.4) µm and cells infiltrated about halfway through the scaffold. HN12 cells did appear to infiltrate more

efficiently in medium scaffolds than HN6 cells did in medium scaffolds. However, infiltration was still greatest for HN6 cells seeded in small fiber diameter scaffolds.

HN6 cells cultured for fourteen days on small fiber scaffolds shows cells migrating throughout the majority of the scaffold (Figure 3.13). Although not as uniform as HN6 cell infiltration on small fiber scaffolds after seven days, there appears to be areas where cells are traveling across the width of the scaffold after fourteen days. When comparing the small fibers to the medium fibers in Figure 3.14, HN6 cells did not infiltrate throughout the scaffold which could again be reflective of the increased thickness and decrease in porosity of the medium fiber scaffold. However, there was more infiltration of HN6 cells after fourteen days compared to seven days in medium size fiber scaffolds.

HN12 cells cultured for fourteen days on small fiber scaffolds remained, for the most part, on the surface of the scaffold (Figure 3.15). Figure 3.16 shows that HN12 cells seeded on medium fiber scaffolds permitted better infiltration than small fiber scaffolds after fourteen days of culture. This was consistent with data collected after seven days as described previously.

Overall, time did not appear to play a big factor in cell infiltration when comparing seven days to fourteen days. Seven days of culturing either HN6 or HN12 cell lines onto small fiber or medium fiber scaffolds was shown to be a sufficient amount of time for cells to infiltrate. Comparing to similar literature that investigated cell infiltration on 3D scaffolds, time points were not taken past seven days [46, 47]. Day seven may also be a more ideal duration for cell seeding because there is a higher risk of cell death the longer they are maintained in culture. Because of this conclusion, treatment of cells with cisplatin was done after seven days of culturing for future studies.

Large fiber scaffolds were fabricated and characterized as previously described, yet were ultimately not used for cell seeding due to difficulty in cryosectioning. However, it appears as though small and medium fiber scaffolds were more appropriate to use for cell seeding because of their smaller thickness and higher porosity. A smaller scaffold thickness, smaller fiber diameters, and a higher percentage in porosity yielded better results for cell infiltration. HN6 cells showed higher infiltration in smaller fiber scaffolds whereas HN12 cells showed higher infiltration in medium fiber scaffolds. The fiber diameters for both the small and medium fibers elicited sufficient cell infiltration because there was an increase in porosity and a larger size to surface area relationship in fibers. In other words, although the fibers are smaller, there is a greater percentage of fiber area present throughout the scaffold [16]. This gives more area for the cells to adhere and therefore generates the opportunity for cells to migrate. Small fibers seeded with HN6 and medium fibers seeded with HN12 show sufficient cell infiltrations, however better infiltration could be achieved with thinner scaffolds.

3.7. Live Dead Analysis of Cisplatin Treated Cells in Fabricated Scaffolds

3.7.1. LIVE/DEAD ASSAY ON CELLS GROWN IN 2D CULTURE

In order to quantify the number of viable cells versus dead cells in the engineered 3D scaffolds a live/dead assay (CMFDA and EthD-1) was used as previously described. CMFDA is a fluorescent dye able to freely pass through cell membranes and it is retained in living cells to enable future microscopic imaging [43]. This was contrasted with EthD-1, a high affinity nucleic acid stain that emits red fluorescence while bound to DNA [44]. Cells were seeded onto 2D glass plates as a pilot study to test the efficacy of the assays. Figure 3.17 shows the results of viable cells seeded on a glass plate. Figure 3.18 shows the result of killing cells

with methanol prior to staining with the live dead assay. Figures 3.17 and 3.18 show the phase image, live assay alone, dead assay alone, and a merge of the phase, live and dead assays. As a result of pilot study shown in Figures 3.17 and 3.18, it was concluded that the live/dead assays were successfully staining live cells and dead cells respectively, therefore the assays could be then transferred to cells grown in 3D scaffolds.

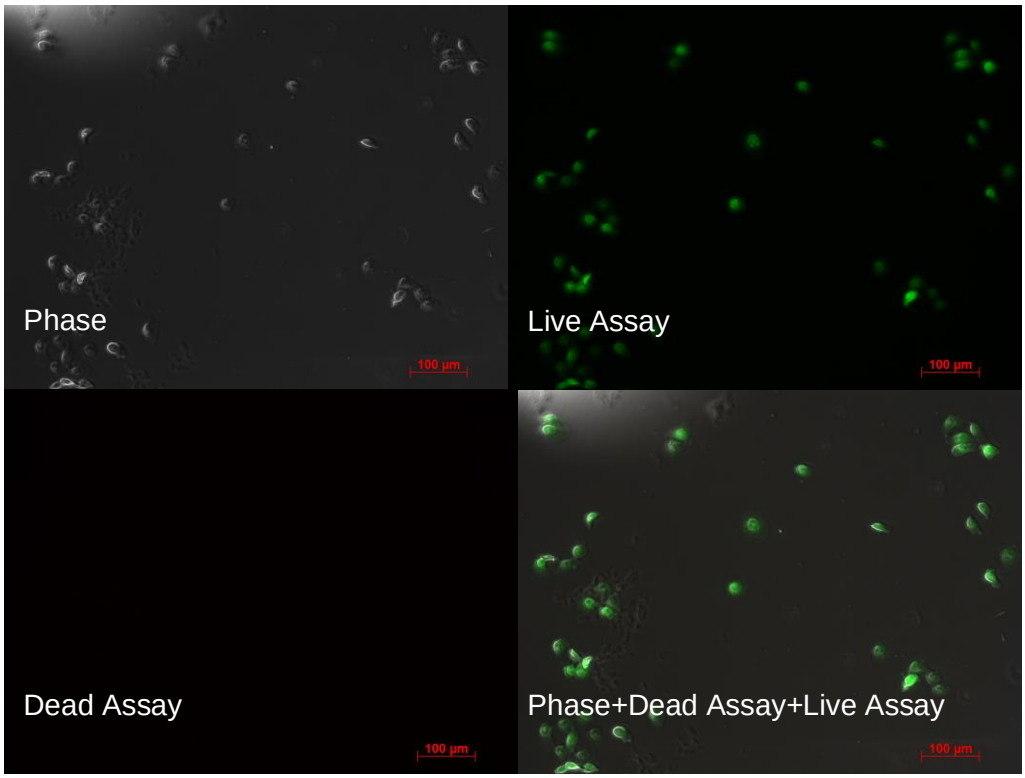

Figure 3.17: Live/dead assays tested on cells grown in 2D to test the efficacy of the assays on live cells.

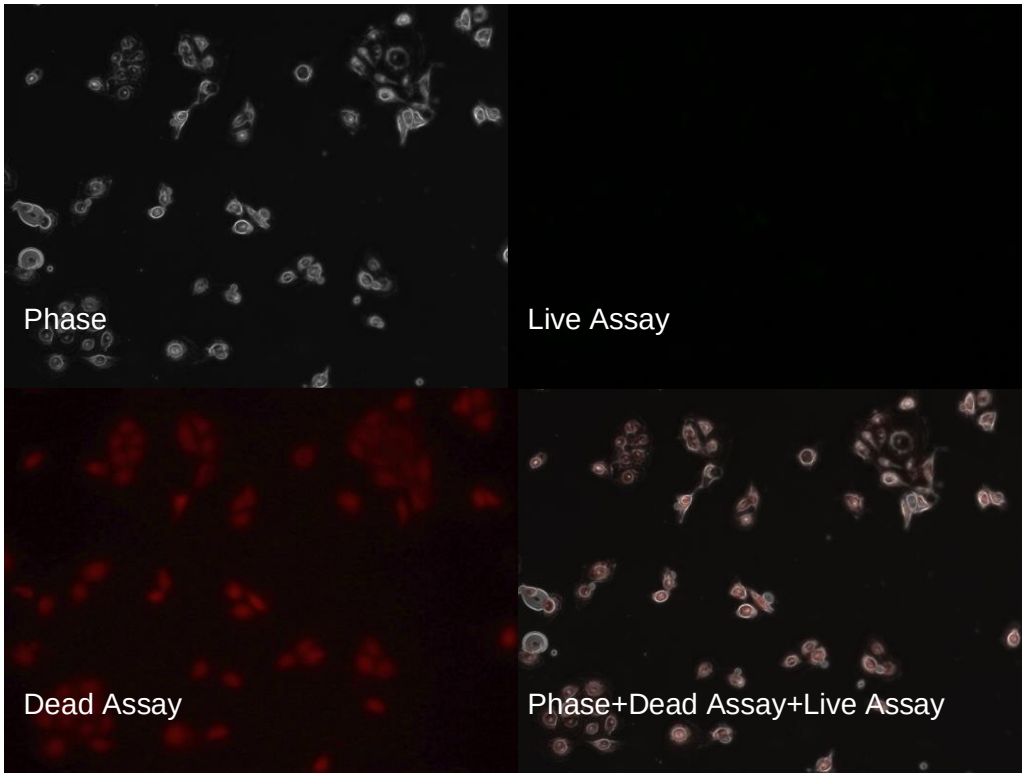

Figure 3.18: Live/dead assays tested on cells grown in 2D to test the efficacy of the assays on dead cells.

3.7.2. DAY 10 WITH NO CISPLATIN TREATMENT

After investigating the infiltration capabilities of HN6 and HN12 in both small and medium fiber scaffolds, it was important to test the viability of these cells in 3D in response to chemotherapeutic drugs. Live/dead assays, as described above, were used to quantify the number of viable cells *versus* the number of dead cells in both fiber size scaffolds after three days of 6 μg/ml cisplatin treatments, which was the IC_{90} determined in 2D culture. Through the live/dead assays the live cells were stained green and the dead cells were stained red and analyzed under fluorescence microscopy. Five random fields were chosen for each cell type seeded on both fiber sizes and from these images, percentages of live cells were calculated. To determine whether cell lines seeded onto the scaffolds were affected by cisplatin, treated samples were compared to controls with identical cell seeding and no cisplatin treatment. Figure 3.19 shows a live/dead analysis of HN6 cells seeded onto small fiber scaffolds after ten days with no cisplatin treatment displaying 53.6% of viable cells. HN6 cells seeded for ten days onto medium fiber scaffolds with no cisplatin treatment were imaged as seen in Figure 3.20 and showed 39.2% of the overall cell populations was viable. Figure 3.21 shows HN12 cells seeded for ten days onto small fiber scaffolds with no cisplatin treatment, where 71.0% cell viability was counted. HN12 cells seeded for ten days on medium fibers with no cisplatin treatment, as seen in Figure 3.22 showed 58.2% of viable cells (Table 3.9).

Table 3.9 Cell viability for untreated scaffolds. (n=5).

	HN12	HN6
Small Fiber Scaffolds	71.0%	53.6%
Medium Fiber Scaffolds	58.2%	39.2%

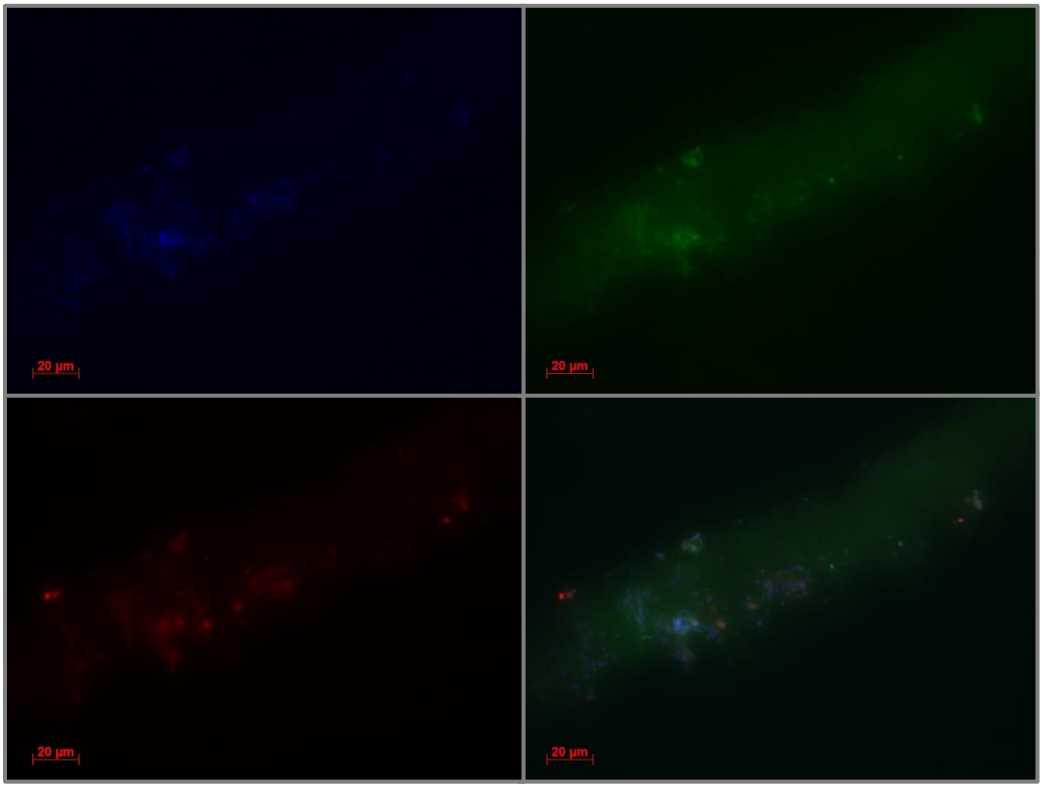

Figure 3.19: Day 10 live/dead analysis of HN6 cells seeded onto small fiber scaffolds with no cisplatin treatment. Cell viability was calculated to be 53.6% (n=5).

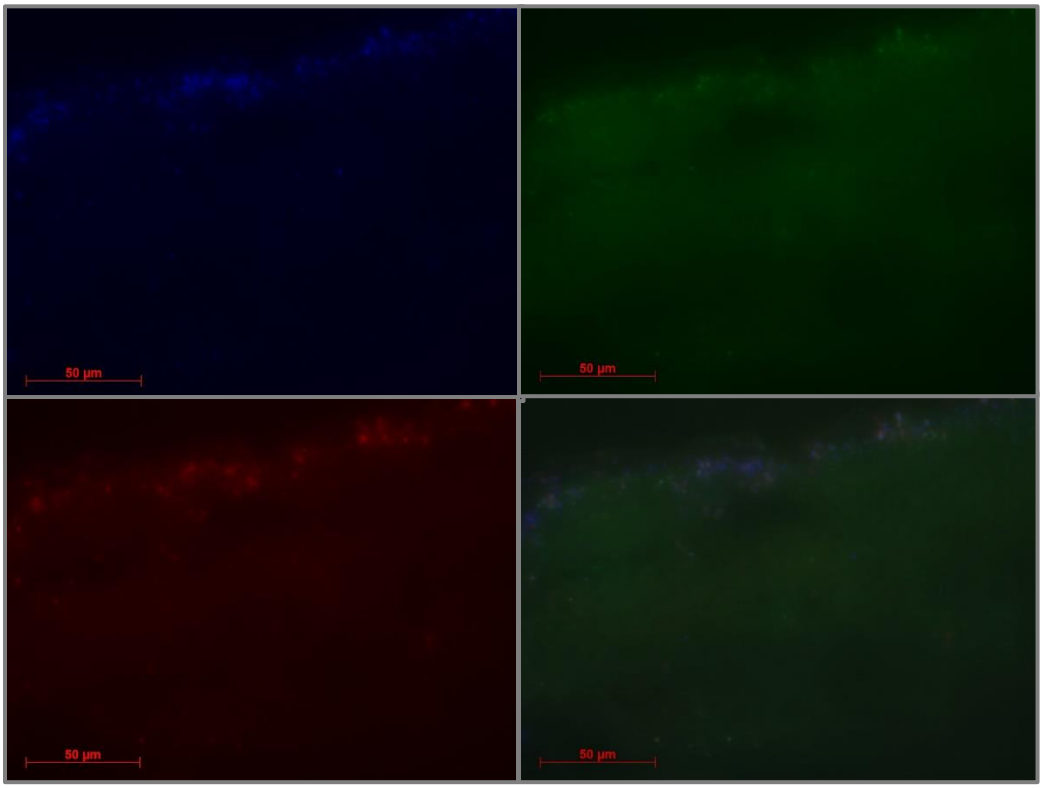

Figure 3.20: Day 10 live/dead analysis of HN6 cells seeded onto medium fiber scaffolds with no cisplatin treatment. Cell viability was calculated to be 39.2% (n=5).

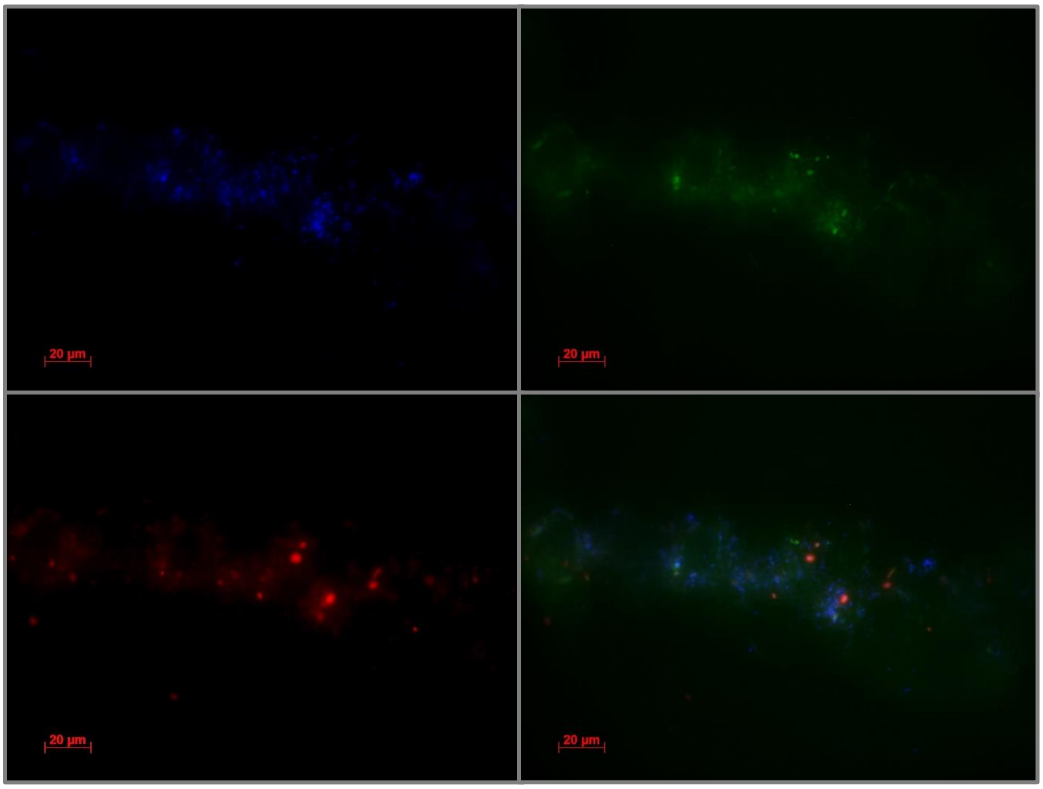

Figure 3.21: Day 10 live/dead analysis of HN12 cells seeded onto small fiber scaffolds with no cisplatin treatment. Cell viability was calculated to be 71% (n=5).

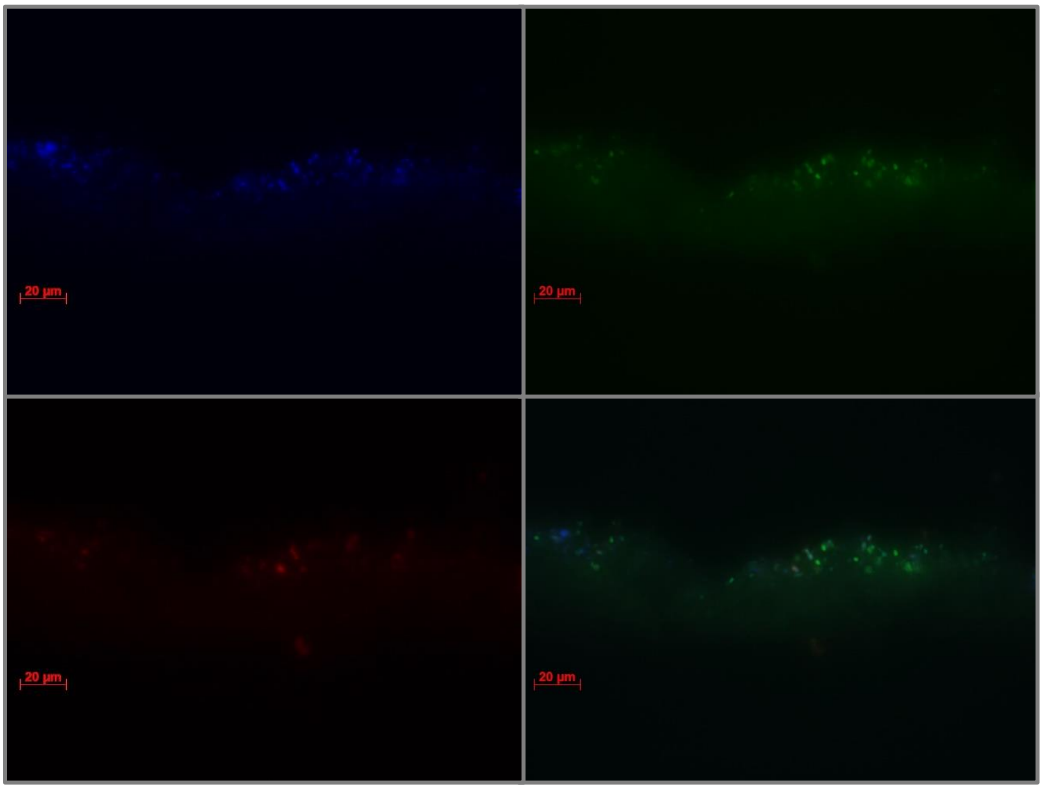

Figure 3.22: Day 10 live/dead analysis of HN12 cells seeded onto medium fiber scaffolds with no cisplatin treatment. Cell viability was calculated to be 58.2% (n=5).

3.7.3. DAY 10 AFTER CISPLATIN TREATMENT

Fabricated scaffolds were seeded with either HN6 or HN12 cells, and after seven days of cell infiltration, were then treated with 6 μg/ml cisplatin. After 72 hours of cisplatin treatment, the live/dead assays were used, as previously described, to quantify the number of viable cells *versus* the number of dead cells. The live/dead assay was used in comparison with the control scaffolds (cells seeded onto scaffolds without cisplatin treatment) in order to quantify the efficacy of the 3D *in vitro* chemotherapeutic drug testing apparatus. Therefore, in order to calculate the number of cells merely affected by cisplatin, the untreated scaffolds were treated as 100% viable in comparison to the treated scaffolds. Figure 3.23 shows the result of HN6 cells seeded onto small fiber scaffolds for seven days followed by three days of cisplatin treatment, where 70.0% cell viability was found when compared to 100% viability in untreated scaffolds. HN6 cells seeded onto medium fiber scaffolds for seven days followed by three days of cisplatin treatment, as seen in Figure 3.24, displayed a cell viability of 15.6%. Figure 3.25 displays HN12 cells seeded on small fiber scaffolds for seven days, where 60.3% cell viability was calculated after three days of cisplatin treatment. HN12 cells seeded onto medium fiber scaffolds after seven days followed by three days of cisplatin treatment, as seen in Figure 3.26, showed 69.4% cell viability (Table 3.10).

Table 3.10 Cell viability for scaffolds treated with 6μg/ml cisplatin. (n=5).

	HN12	HN6
Small Fiber Scaffolds	60.3%	70.0%
Medium Fiber Scaffolds	69.4%	15.6%

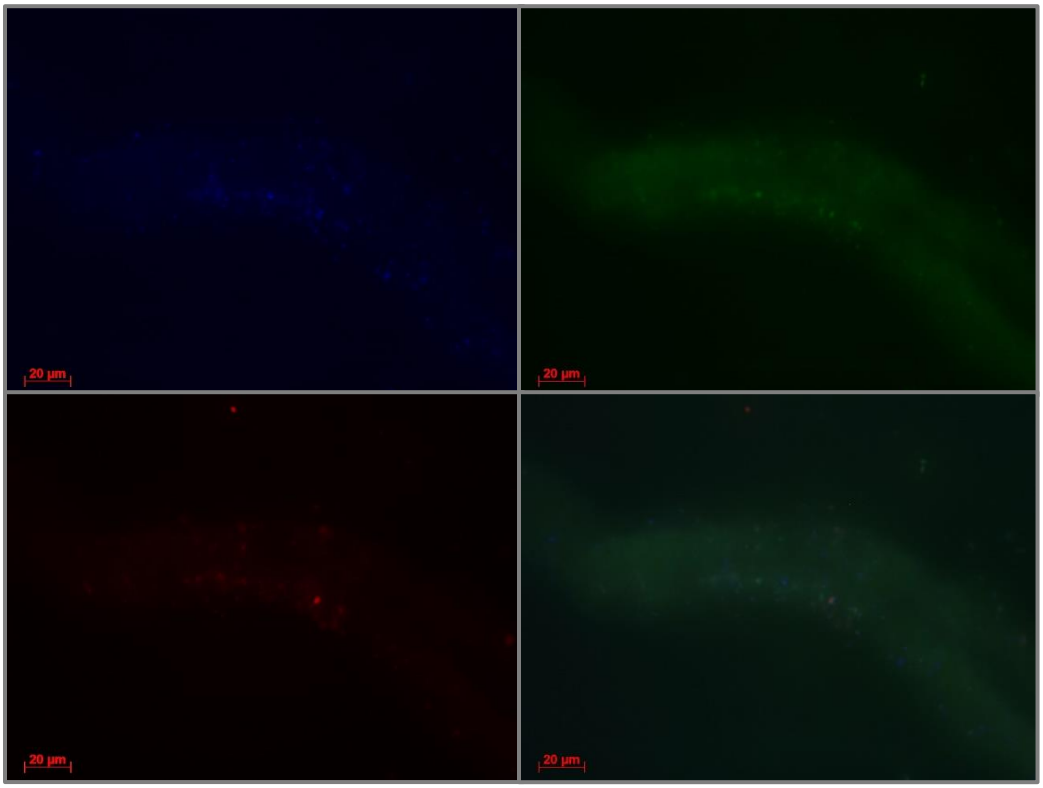

Figure 3.23: Day 10 live/dead analysis of HN6 cells seeded onto small fiber scaffolds after three days of cisplatin treatment. Cell viability was calculated to be 70.0% (n=5).

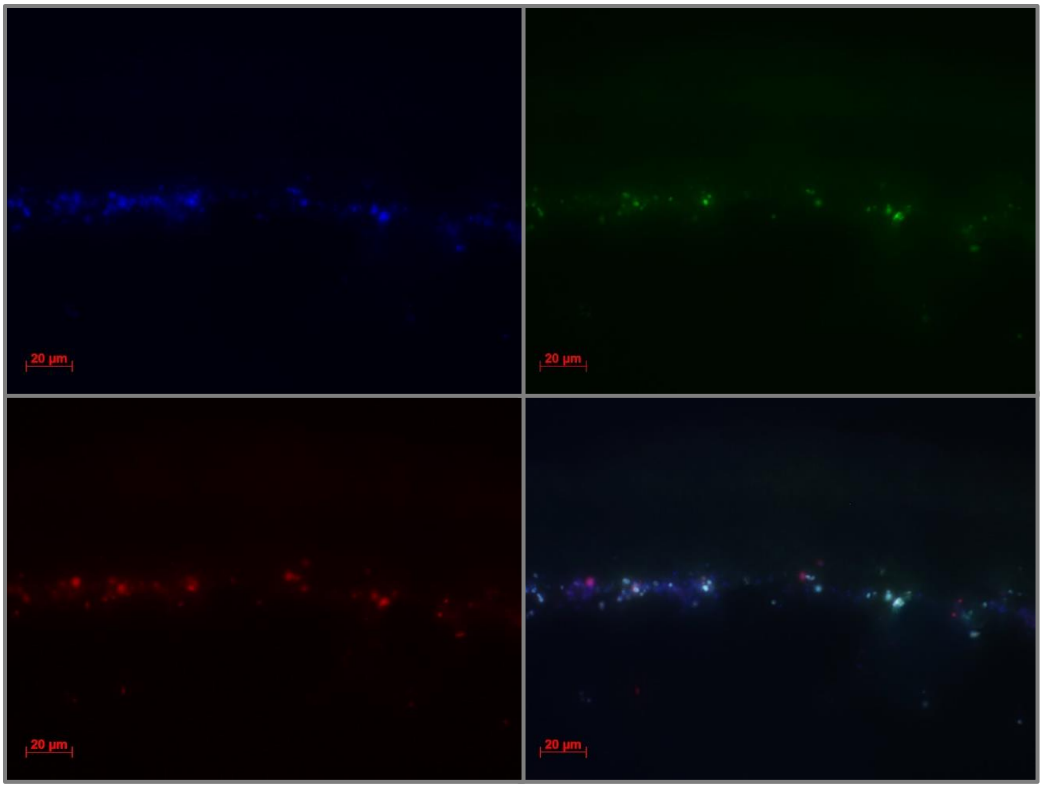

Figure 3.24: Day 10 live/dead analysis of HN6 cells seeded onto medium fiber scaffolds after three days of cisplatin treatment. Cell viability was calculated to be 15.6% (n=5).

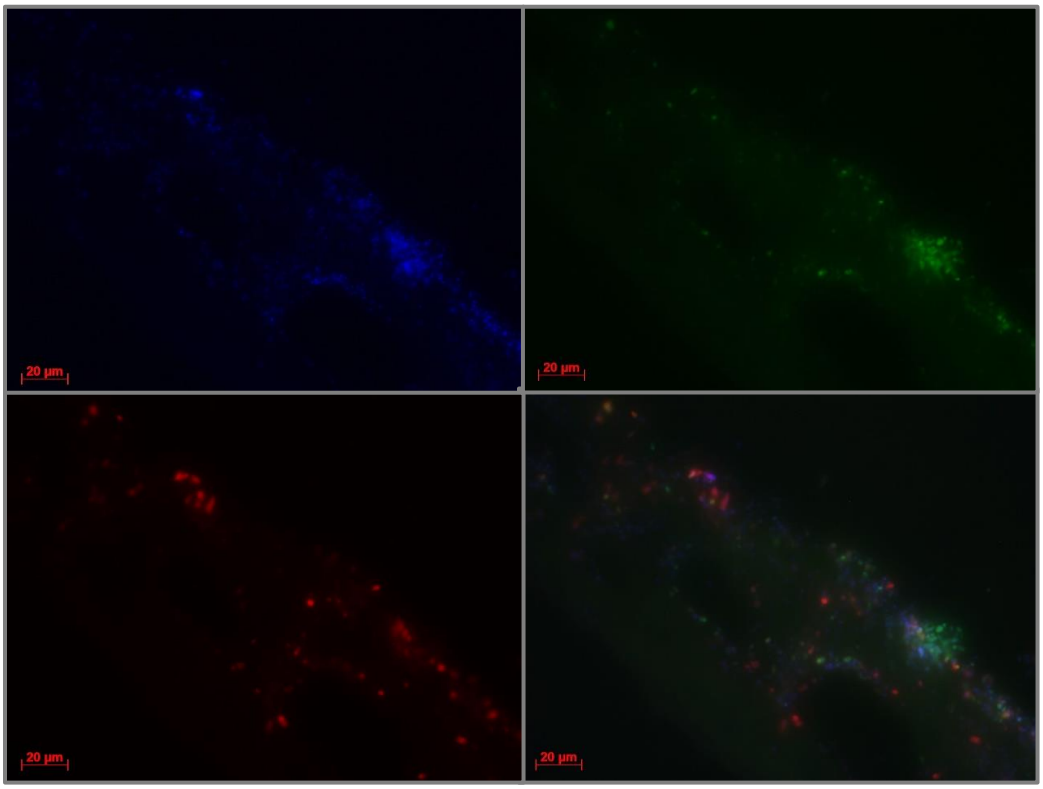

Figure 3.25: Day 10 live/dead analysis of HN12 cells seeded onto small fiber scaffolds after three days of cisplatin treatment. Cell viability was calculated to be 60.3% (n=5).

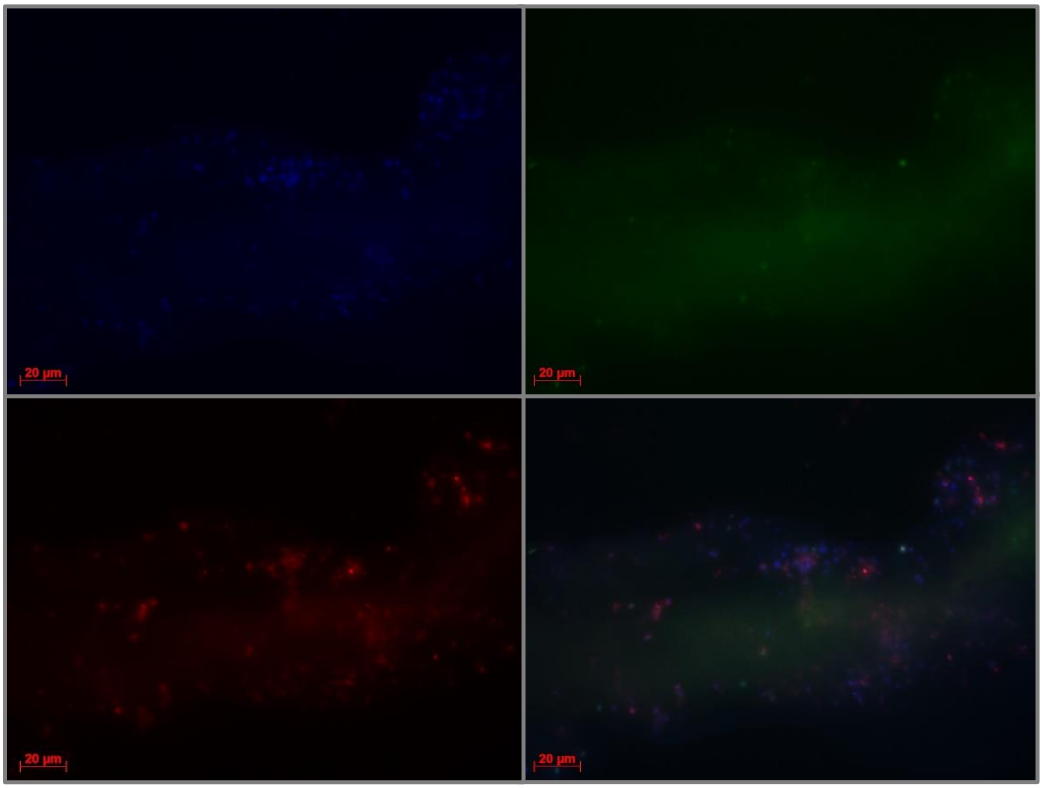

Figure 3.26: Day 10 live/dead analysis of HN12 cells seeded onto medium fiber scaffolds after three days of cisplatin treatment. Cell viability was calculated to be 69.4% (n=5).

3.8. Live Dead Analysis of Treated Cells in Fabricated Scaffolds Conclusions

HN6 and HN12 cell lines were seeded onto both small and medium fiber scaffolds for seven days and then were tested for cell viability. Half of the scaffolds were treated with the IC_{90} concentration of cisplatin, as determined in 2D culture, for 72 hours while half of the scaffolds were re-fed with culture media for 72 hours to compare the efficacy of the drug on the two different cell lines seeded onto the two different fiber size scaffolds. As a result, for each condition, cisplatin treatment was effective for killing the total number of viable cells. However, the efficacy of cisplatin treatment varied between different conditions. Initial cell viability percentages were determined for each untreated scaffold. These initial viability percentages were then taken as 100% viability of cells that have not been treated by cisplatin in order to calculate cell viability post cisplatin treatment. The 100% cell viability for untreated scaffolds was considered in order to take out all other variables, except for cisplatin treatment, that may cause cell death.

HN6 cells seeded for ten days onto small fiber scaffolds untreated showed 53.6% cell viability (Figure 3.19, Table 3.9). This data suggests that about half of the HN6 seeded on to small fiber scaffolds remained viable after ten days without any cisplatin treatment. Several possibilities could account for the 46.4% HN6 cell death on untreated small fiber scaffolds including ten days being too long to maintain sufficient cell viability, HN6 cell sensitivity to PLLA, or a harsh environment for adequate nutrient exchange in porous 3D scaffolds. When comparing viability of HN6 cells on small fiber scaffolds between untreated and those treated with cisplatin, 100% to 70.0% respectively, there was a drop in 30% cell viability (Figures 3.19 and 3.23, Tables 3.9 and 3.10). This confirmed that cisplatin was effective in killing 30% HN6 cells on small fiber scaffolds when compared to untreated samples. However, it is apparent that

6 μg/ml cisplatin was unable to kill 90% of HN6 cells in the small fiber scaffold as it was shown to only kill 30%. These data confirm reports in the literature suggesting cancer cells show resistance to chemotherapeutic drugs when seeded in a 3D microenvironment *versus* a 2D microenvironment. HN6 cells seeded onto small fiber 3D scaffolds showed a resistance to the IC_{90} value of cisplatin used to kill HN6 cells in 2D (Figures 3.20 and 3.3). Comparing the two conditions, 6 μg/ml of cisplatin killed 89% of HN6 cells seeded on 2D tissue culture plates and 30% of HN6 cells seeded onto small fiber scaffolds. Overall, there was a 59% increase in viable HN6 cells in small fiber scaffolds than from HN6 cells in 2D culture. As seen previously in Figures 3.9 and 3.13, HN6 cells infiltrated most efficiently in small fiber scaffolds, which may accurately mimic an *in vivo* tumor. These data suggest that the 3D arrangement of HN6 cells could enhance cell survival where HN6 cells become more resistant to the IC_{90} dose of cisplatin successful for killing HN6 cells treated in 2D.

HN6 cells seeded onto medium fiber scaffolds for ten days with no cisplatin treatment showed 39.2% viability (Figure 3.20, Table 3.9). Similar possibilities, as listed previously, could have played a role in killing 60.8% of HN6 cells on medium fibers including harsh cell culture environments and ten days being too long for adequate cell viability. When comparing untreated HN6 cells on small fibers to untreated HN6 on medium fibers there is a decrease of 14.4% cell viability. During infiltration studies, it was found that HN6 cells tended to form a monolayer on top of medium fiber scaffolds (Figures 3.10 and 3.14). This lack of HN6 cell infiltration in medium fiber scaffolds could account for less cell adhesion and, therefore, an increase in cells dying off or being suctioned off while replacing media. Medium fiber scaffolds seeded with HN6 cells that were treated with 6 μg/ml of cisplatin showed 15.6% viability (Figure 3.24, Table 3.10). When comparing medium fiber scaffolds seeded with HN6 cells, treated with cisplatin

versus untreated, there was a decrease in viability by 84.4%. A dose of 6 μg/ml was effective in killing 85% of HN6 cells in medium fiber scaffolds which disagrees with the assumption that cancer cells become resistant to chemotherapeutics in 3D culture. Comparing HN6 in 2D to HN6 cells on 3D medium fiber scaffolds shows similar results, 9% viability and 15% viability respectively (Figures 3.3 and 3.24, Table 3.10). These data suggests that seeding HN6 cells onto medium fibers treated with cisplatin will reproduce similar cytotoxicity results to HN6 cells treated with cisplatin in 2D. Because of cell infiltration previously found, Figures 3.10 and 3.14, it is possible that HN6 cells seeded onto medium fibers represent an identical monolayer of cells, like those seeded in 2D, and is does not accurately represent a 3D tumor model.

Untreated HN12 cells seeded on small fibers for ten days resulted in the highest initial viability of 71% (Figure 3.21). As previously stated, 29% of HN12 cells seeded on small fibers could have died after ten days because of several possibilities such as culture time or overpopulation of cells. Comparing initial viability of HN12 to HN6 cells in untreated scaffolds, HN12 cells were more viable on small fibers. This could be due to HN12 cells being more tumorigenic and invasive, and less sensitive to fabricated microenvironments. Small fiber scaffolds seeded with HN12 cells that were treated with cisplatin showed 60.3% viability (Figure 3.25, Table 3.10). There was a decrease in viability by 39.7% because of the presence of cisplatin. Table 3.10 shows that 6 μg/ml of cisplatin is effective in killing 39.7% of HN12 cells seeded in small fibers rather than the 99% of HN12 cells killed when seeded in 2D as seen in Table 3.4. These data suggest that there is a resistance to cisplatin when transitioning HN12 from 2D to 3D microenvironments. Figure 3.11 shows a fair amount of cell infiltration inferring a 3D arrangement of HN12 cells in small fibers which could result in a resistance to cisplatin treatment.

Figure 3.22 shows a viability of 58.2% of untreated HN12 cells seeded onto medium fibers after ten days (Table 3.9). This viability is lower when compared to HN12 cells seeded onto small fibers, as previously described, which could be a result of cells being introduced to a harsher environment. According to Table 3.9 it can be concluded, that for both HN12 and HN6, cells are less viable in medium fiber size scaffolds. HN12 cell viability decreased by 12.8%, whereas HN6 cell viability decreased by 14.4% when transitioning from seeding on small fibers to medium fibers. Both cell lines may prefer the smaller diameter because there is more surface area for adhesion, a higher porosity percentage for nutrient exchange, and more binding sites for growth factors which would all enhance the viability of cells.

Figure 3.16 displays treated HN12 cells on medium fibers to be 69.4% viable, which was similar to treated HN12 cells on small fibers (Tables 3.9, 3.10). Cisplatin was effective in killing 30.6% of HN12 cells in medium fibers rather than 99% of HN12 cells killed when seeded in 2D, as seen in Table 3.4. These data suggest that there is a resistance to cisplatin when transitioning HN12 from 2D to 3D microenvironments. Figures 3.12 and 3.16 display a fair amount of HN12 cell infiltration in medium fibers suggesting a 3D arrangement that might increase resistance to cisplatin treatment.

It has been concluded that HN12 show a greater resistance to IC90 values of cisplatin than HN6. It was also shown that HN12 cells were able to infiltrate throughout both scaffold types, whereas HN6 cells were only able to infiltrate through the small fibers (however, they formed a monolayer on top of the medium fiber scaffolds). Primary HN12 tumor cells are epithelial, yet, through previous work in the lab it has been shown that HN12 cells undergo an epithelial to mesenchymal transition during tumorigenesis [6]. This process can occur during cancer progression, where epithelial cells 1) lose their junctions and apical-basal polarity; 2)

reorganize their cytoskeleton; and 3) undergo a change in the signaling programs that define cell shape and reprogram gene expression. All of these processes increase the motility of individual HN12 cells and produces a more invasive phenotype. Specifically, epithelial actin architecture reorganizes, and cells acquire motility and invasive capacities by forming lamellipodia, filopodia, and invadopodia- which allow for the progression of cancer cells, and enhance cell resistance to apoptosis. Finding that HN12 cells undergo endothelial to mesenchymal transition during tumorogenisis- and therefore have greater mobility- is consistent with the conclusion that HN12 cells appeared more invasive, and were able to infiltrate better throughout both scaffolds [50].

Electrospun scaffolds allow for a porous environment to promote cell infiltration; however, upon the introduction of media, wetting the scaffolds can cause contraction and densification throughout. Previous studies have shown that this densification should not affect cellular penetration and migration into the scaffolds, although it can reduce permeability. This reduction in permeability throughout the scaffolds can result in decreased nutrient and waste diffusion. Lack of proper diffusion can account for cancer cell death in PLLA scaffolds despite the absence of anticancer drugs because of a lack of nutrients and a higher incidence of hypoxia induced apoptosis [49].

Although it was shown through experimentation, it is apparent that cell adhesion decreased as fiber diameter increased. This, as explained previously, is due in part to a more localized area provided for cell adhesion, and a closer network of cell-cell interaction which promotes cell growth. The small and medium sized fibers better resembled the micro-environment of HN12 cells *in*-vivo- which would allude to small and medium fibers providing better cell attachment for HN12 and HN6 in tissue engineered scaffolds. HN6 cells in particular

were trending towards greater cell death as fiber size increased, so it could be inferred that larger fibers would be a less desirable micro-environment for HN6 cell viability. Although not included in this study's results, fluorescent images of large fibers seeded with both HN6 and HN12 were taken only to show that very little cell attachment had occurred.

Chapter 4 Future Work

Several different parameters were investigated while designing an ideal 3D scaffold used for testing *in vitro* chemotherapeutic drug efficacy. As previously described, it was found that a smaller fiber size gave opportunity for a higher surface area of fibers and porosity and increased cell infiltration. Therefore, scaffolds characterized as small and medium fiber scaffolds were successfully used for seeding of both HN6 and HN12 cells. For future studies of drug efficacy in these cell lines with PLLA engineered scaffolds, HN6 should be seeded onto smaller fiber scaffolds whereas HN12 cells should be seeded onto small or medium size scaffolds, as previously shown. No significant difference was found between cell infiltration in seven days and fourteen days; therefore, for future work, cells should be cultured for only seven days. A decrease in cell culture duration in 3D scaffolds will minimize possible cell death and increase accuracy of drug testing. It might be important to see if a shorter time point could be used that shows similar infiltration, such as four days, that would elicit similar cell infiltration. Future engineered scaffolds should be designed to be thinner in order to ensure 100 percent cell infiltration and best represent 3D *in vivo* HNSCC tumors. Figures 3.9, 3.12, 3.13, and 3.16 all appear to have fair cell infiltration throughout the scaffold ranging from about 25% to about 90% of the scaffold thickness. In order to ensure both HN6 and HN12 cells infiltrate throughout the entire scaffold, a smaller volume of PLLA solution in HFP could be electrospun. For the fabrication of each scaffold in these studies, 1 ml of solutions was electrospun, whereas in the

future a reduced volume such as 0.75 ml may allow fabrication of thinner scaffolds that permit higher cell infiltration. According to our results, future fabricated scaffolds designed to have thicknesses of about 40 μm could induce ideal cell infiltration for HN6 cells seeded on small fibers and HN12 cells seeded on small and medium fibers.

Four different conditions were investigated while designing and implementing an *in vitro* 3D cancer model for chemotherapeutic drug testing including HN6 cells seeded on small or medium fibers, and HN12 cells seeded on small or medium fibers. As the results have shown, it is apparent that HN6 cells are not as viable as HN12 cells in fabricated scaffolds. Therefore, it may be more beneficial to consider more invasive cell lines that are similar to HN12. If HN6 cells are to be used in the future, consider seeding them on smaller fibers as they have proved to show better infiltration and viability. It also may be more beneficial for HN12 cells to just be seeded onto small fiber scaffolds, as the data have shown that both cell lines are less viable in medium fiber scaffolds (Table 3.9). Each of these conditions was treated with 6 μg/ml of cisplatin, which was found to be an accurate IC_{90} concentration for both cell lines seeded in 2D. The results of these treated scaffolds were then compared to each other as well as to untreated control scaffolds seeded for the same duration of ten days. For overall cisplatin treatment testing, the number of days for cell seeding could be reduced. It is possible that this is the main cause for untreated cells not being closer to 100% viable. As recommended previously, seeding for 4 days may allow enough time for cells to infiltrate and minimize amount of cell death. After day 4, the cells could then be treated with cisplatin for 72 hours, totaling 7 days of cell seeding rather than 10 days. It might also be important to look into blending natural ECM components into the scaffolds to increase cell adhesion. Another consideration is to introduce air flow during electrospinning to fabricate more porous scaffolds, if a lack of nutrient exchange is a concern.

Increasing treatments of cisplatin could then be administered to each condition, much like those seen in Tables 3.3 and 3.4. From there it would then be possible to identify an IC_{90} concentration for cisplatin in 3D and compare that value to the IC_{90} concentrations found in 2D cell seeding. The IC_{90} concentration found while testing cisplatin on HN6 and HN12 in 3D culture environments could then be compared to clinical doses of cisplatin to determine the efficacy of the *in vitro* engineered 3D cancer model.

Drug permeability through the scaffold was not specifically measured. Future studies will need to be done in order to determine the exact permeability; however, based on the images produced by the live/dead assay and the scaffolds' porosity, several inferences can be drawn. First, as shown in Figures 3.23-3.26, when the live/dead assays were conducted on the cancer-seeded scaffolds treated with cisplatin, cell death can be observed throughout the scaffolds. While such an analysis is by no means conclusive, it does at least suggest that the drugs were able to spread throughout the two types of scaffolds. Moving forward, more studies will need to be done to determine the exact permeability of cisplatin in PLLA scaffolds with identical scaffold parameters.

It has been concluded that both cancer cell lines develop a resistance to cisplatin when seeded in a 3D culture. Although, it became apparent that cisplatin was successful in killing a percentage of cells in each fiber size scaffolds; though a quantitative measurement of how effectively the drug was permeating through the scaffold is undetermined. For future studies it would be important to conduct experiments similar to Sell et al. in order to calculate the permeability of the drug inside both the small fiber and the medium fiber scaffolds [49]. Identical scaffolds could be designed with the same thickness, porosity, and fiber diameter to test how much of the drug concentration can travel throughout the scaffold. A flowmeter could be

used that allows a specific amount of fluid to pass through a fixed electrospun scaffold over time. By using a similar method as Sell et al., a known amount of liquid can be poured into a filling port where it is then pushed though through a glass tubing where the electrospun is encased. The scaffolds would be punched into the same diameter shapes used for cell seeding and would be vacuumed inside the flow meter to eliminate any other external variables. These scaffolds could then be tightly compressed in the apparatus to ensure that the liquid will perfuse through a specific area of the scaffold. The perfused liquid would flow through the scaffold past a metal screen and into a beaker. Calculations could then be made in order to compare the amount of starting fluid to the amount of resulting perfused fluid. Prior experiments have tested the flowmeter by perfusing water through the scaffolds, but in order to test cisplatin permeability it would be useful to perfuse the scaffolds with a liquid of identical viscosity- or even the cisplatin solution itself. A dye, such as food coloring, could then be added to the solution in order to visualize where perfusion occurs within the scaffolds. After gathering these data, it could then be compared to the porosity calculations and the live/dead analyses previously determined in order to conclude the extent to which cisplatin perfuses through electrospun PLLA scaffolds of small and medium fiber types.

Future scaffolds could be electrospun with PLLA in combination with other natural polymers. 3D matrices formed with the combination of polymer and natural polymer (ie. laminin, collagen, gelatin) have an advantage because biological sources derived from the ECM provide mechanical cues that affect cell behavior, gene expression, and drug sensitivity. The inclusion of ECM molecules can initiate signal cascades in tumor cells and function as bio-active molecules, such as ligands. These ligands can be sued for a number of cell surface receptors and integrins which could activate downstream target proteins that can activate various signaling

pathways in cancer cells such as angiogenesis, cancer cell motility, and drug sensitivity. For example, Collagen I can interact with integrins and affect gene expression; which in turn allows for the production of enzymes that degrade ECM components allowing for cancer invasion, cell sensitivity to cancer drugs, cell proliferations, and migration. In short, the inclusion of a natural polymer blend in the PLLA electrospun scaffolds could better mimic *in-vivo* ECM of HN12 and HN6 cells. This more natural ECM may allow the cells to better mimic their response to cisplatin *in vivo* and represent appropriate drug sensitivity experienced in the body [22].

Bibliography

[1] Crozier, Emily, and Baran D. Sumer, MD. "Head and Neck Cancer." *Medical Clinics of North America* 94.5 (2010): 1031-046. Print.

[2] Lin, Charles J., Jennifer R. Grandis, Thomas E. Carey, Susanne M. Gollin, Theresa L. Whiteside, Wayne M. Koch, Robert L. Ferris, and Stephen Y. Lai. "Head and Neck Squamous Cell Carcinoma Cell Lines: Established Models and Rationale for Selection." *Head & Neck* 29.2 (2007): 163-88. Web.

[3] Zhang, Xiao-Hui. "Why Cancer Cells Metastasize?" *Medical Hypotheses* 80.5 (2013): 669-71. Print.

[4] "Head and Neck Cancers - National Cancer Institute." *Head and Neck Cancers - National Cancer Institute*. N.p., n.d. Web. 19 Feb. 2014.

[5] Day, Terry A., Angela Chi, Brad Neville, and James R. Hebert. "Prevention of Head and Neck Cancer." *Current Oncology Reports* 7.2 (2005): 145-53. Print.

[6] Bulysheva, Anna A., Yeudall, W. Andrew, Bowlin, Gary L. "Three Dimensional *In Vitro* Model of Head and Neck Squamous Cell Carcinoma." Virginia Commonwealth University School of Engineering. May, 2012

[7] Oral Cavity and Oropharyngeal Cancer. Available at: http://www.cancer.org/acs/groups/cid/documents/webcontent/003128-pdf.pdf. Accessed 3/3, 2014

[8] "Models of Cancer." *Nature.com*. Nature Publishing Group, n.d. Web. 17 Mar. 2014.

[9] Cheon, Dong-Joo, and Sandra Orsulic. "Mouse Models of Cancer." *Annual Review of Pathology: Mechanisms of Disease* 6.1 (2011): 95-119. Print.

[10] Lin, C. J., Grandis, J. R., Carey, T. E., Gollin, S. M., Whiteside, T. L., Koch, W. M., ... Lai, S. Y. (2007, 12). Head and neck squamous cell carcinoma cell lines: Established models

and rationale for selection. *Head & Neck*, *29*(2), 163-188. doi: 10.1002/hed.20478

[11] Corlan AD. Medline (PubMed) trend. Available at: http://dan.corlan.net/medline-trend.html. Accessed 3/18, 2014.

[12] "Genes and Mapped Phenotypes." *National Center for Biotechnology Information*. U.S. National Library of Medicine, n.d. Web. 18 Mar. 2014.

[13] Trask, D. K. "Keratins as Markers That Distinguish Normal and Tumor-Derived Mammary Epithelial Cells." *Proceedings of the National Academy of Sciences*87.6 (1990): 2319-323. Print.

[14] Alberts, Bruce. "The Extracellular Matrix of Animals." *The Extracellular Matrix of Animals*. U.S. National Library of Medicine, 18 Feb. 0000. Web. 19 Mar. 2014.

[15] Ziober, Amy F., Erica M. Falls, and Barry L. Ziober. "The Extracellular Matrix in Oral Squamous Cell Carcinoma: Friend or Foe?" *Head & Neck* 28.8 (2006): 740-49. Print

[16] Lannutti, J., D. Reneker, T. Ma, D. Tomasko, and D. Farson. "Electrospinning for Tissue Engineering Scaffolds." *Materials Science and Engineering: C* 27.3 (2007): 504-09.

[17] Neville, Brad W., DDS, and Terry A. Day, MD. "CA: A Cancer Journal for Clinicians Volume 52, Issue 4, Article First Published Online: 23 FEB 2009." *Oral Cancer and Precancerous Lesions*. CA: A Cancer Journal for Clinicians, July-Aug. 2002. Web. 20 Mar. 2014.

[18] Wang, Jing, Wenli Zhu, Hongtao Zhang, and Chul B. Park. "Continuous Processing of Low-density, Microcellular Poly(lactic Acid) Foams with Controlled Cell Morphology and Crystallinity." *Chemical Engineering Science* 75 (2012): 390-99. Print.

[19] Hu, Jian, Tongping Zhang, Minggang Gu, Xing Chen, and Jianming Zhang. "Spectroscopic Analysis on Cold Drawing-induced PLLA Mesophase." *Polymer*53.22 (2012): 4922-926.

[20] Lin Xiao, Bo Wang, Guang Yang, and Mario Gauthier (2012.) Poly(Lactic Acid)-Based

Biomaterials: Synthesis, Modification and Applications, Biomedical Science, Engineering and Technology, Prof. Dhanjoo N. Ghista (Ed.), ISBN: 978-953-307-471-9, InTech, Available from: http://www.intechopen.com/books/biomedical-science-engineering-and-technology/poly-lactic-acid-based-biomaterials-synthesis-modifaction-and-applications

[21] The Editors of Encyclopædia Britannica. "Young's Modulus (physics)." *Encyclopedia Britannica Online*. Encyclopedia Britannica, n.d. Web. 30 Mar. 2014.

[22] Gurski, Lisa A., BS, Nicholas J. Petrelli, MD, Xinqiao Jia, PhD, and Mary C. Farach-Carson, PhD. "3D Matrices for Anti-Cancer Drug Testing and Development." *Oncology Issues: From Research to Practice* (2010): 20-25. Web. <https://accc-cancer.org/oncology_issues/articles/janfeb10/JF10-Research.pdf>.

[23] Hongisto, Vesa, Sandra Jernstrã¶M, Vidal Fey, John-Patrick Mpindi, Kristine Kleivi Sahlberg, Olli Kallioniemi, and Merja Perã¤Lã¤. "High-Throughput 3D Screening Reveals Differences in Drug Sensitivities between Culture Models of JIMT1 Breast Cancer Cells." Ed. Mariaâ A. Deli. *PLoS ONE* 8.10 (2013): E77232. Print.

[24] "Cancer Drug Information." *Paclitaxel*. N.p., 05 Oct. 2006. Web. 01 Apr. 2014. <http://www.cancer.gov/cancertopics/druginfo/paclitaxel>.

[25] "Cisplatin (Intravenous Route)." *Proper Use*. N.p., n.d. Web. 11 Apr. 2014. http://www.mayoclinic.org/drugs-supplements/cisplatin-intravenous-route/proper-use/drg-20062953

[26] "Cisplatin." *American Cancer Society*. N.p., 14 Jan. 201. Web. 11 Apr. 2014.

[27] Horning, Jayme L., Sanjeeb K. Sahoo, Sivakumar Vijayaraghavalu, Sanja Dimitrijevic, Jaspree K. Vasir, Tapan K. Jain, Amulya K. Panda, and Vinod Labhasetwar. "3-D Tumor

Model For Evaluation of Anticancer Drugs." *Molecular Pharmaceutics* 5.5 (2008): 849-62. Print.

[28] Chen, Ming, Prabir K. Patra, Steven B. Warner, and Sankha Bhowmick. "Role of Fiber Diameter in Adhesion and Proliferation of NIH 3T3 Fibroblast on Electrospun Polycaprolactone Scaffolds." *Tissue Engineering* 13.3 (2007): 579-87. Print.

[29] "WST-1 Cell Proliferation Assay Kit." *Cayman Chemical New Products*. N.p., n.d. Web. 02 May 2014.

[30] Xu, Leyuan, Yang, Hu, PhD, Gary L. Bowlin, PhD, and W. Andrew Yeudall, PhD, DDS. *Semi-Interpenetrating Network Gelatin Fiber Sca*. Thesis. Virginia Commonwealth University, 2013. N.p.: n.p., n.d. Print.

[31] "Taxol (Paclitaxel) Drug Information: Description, User Reviews, Drug Side Effects, Interactions - Prescribing Information at RxList." *RxList*. N.p., n.d. Web. 02 May 2014.

[32] "Cisplatin (Cisplatin Injection) Drug Information: Description, User Reviews, Drug Side Effects, Interactions - Prescribing Information at RxList."*RxList*. N.p., n.d. Web. 02 May 2014.

[33] Boland, Eugene D., Todd A. Telemeco, David G. Simpson, Gary E. Wnek, and Gary L. Bowlin. "Utilizing Acid Pretreatment and Electrospinning to Improve Biocompatibility of Poly(glycolic Acid) for Tissue Engineering." *Journal of Biomedical Materials Research* 71B.1 (2004): 144-52. Print.

[34] Jamur, MC. "Methods in Molecular Biology." *Permeabilization of Cell Membranes* 6th ser. 588.63 (2010): n. pag. *PubMed*. Web. 3 May 2014.

[35] Król, M., KM Pawłowski, Majchrzak K, Szyszko K, and Motyl T. "Why Chemotherapy Can Fail?" *Polish Journal of Veterinary Sciences* 13.2 (2010): 399-406. *PubMed*. Web.

19 May 2014.

[36] Rona, Zoltan, MD. "The Failure of Chemotherapy." *Alive: Your Complete Source for Natural Health and Wellness*. ALIVE PUBLISHING GROUP, Mar. 2000. Web.

[37] Gardner, Amanda. "Head & Neck Cancer, Chemo & Radiation." *MedicineNet*. MedicineNet, Inc., 2004. Web. 19 May 2014.

[38] Bhardwaj, Nandana, and Subhas C. Kundu. "Electrospinning: A Fascinating Fiber Fabrication Technique." *Biotechnology Advances* 28.3 (2010): 325-47. Web.

[39] "How Can I Determine an EC90 (or Any EC Value Other Than EC50)?" *GraphPad.*

[40] Wang, Xueqing, Lingya Pan, Ning Mao, Lifang Sun, Xiangjuan Qin, and Jie Yin. "Cell-cycle Synchronization Reverses Taxol Resistance of Human Ovarian Cancer Cell Lines." *Cancer Cell International* 13.1 (2013): 77. Web.

[41] Fong, H. I., and D. H. Reneker. "Beaded Nanofibers Formed during Electrospinning." *Polymer 40* (1999): 4585-592. *Elsevier*. Web.

[42] Loh, Qiu Li, and Cleo Choong. "Three-Dimensional Scaffolds for Tissue Engineering Applications: Role of Porosity and Pore Size." *Tissue Engineering Part B: Reviews* 19.6 (2013): 485-502. Web.

[43] "CellTracker™ Green CMFDA." - *Life Technologies*.

[44] "Ethidium Homodimer-1 (EthD-1)." - *Life Technologies*. Web.

[45] Welters, M. JP, A. MJ Fichtinger-Schepman, R. A. Baan, A. J. Jacobs-Bergmans, A. Kegel, W. JF Van Der Vijgh, and B. JM Braakhuis. "Pharmacodynamics of Cisplatin in Human Head and Neck Cancer: Correlation between Platinum Content, DNA Adduct Levels and Drug Sensitivity in Vitro and in Vivo." *British Journal of Cancer* 79.1 (1999): 82-87.

[46] Blakeney, Bryan A., Ajay Tambralli, Joel M. Anderson, Adinarayana Andukuri, Dong-Jin Lim, Derrick R. Dean, and Ho-Wook Jun. "Cell Infiltration and Growth in a Low Density, Uncompressed Three-dimensional Electrospun Nanofibrous Scaffold." *Biomaterials* 32.6 (2011): 1583-590. Web.

[47] Li, Linhao, Yuna Qian, Chao Jiang, Yonggang Lv, Wanqian Liu, Li Zhong, Kaiyong Cai, Song Li, and Li Yang. "The Use of Hyaluronan to Regulate Protein Adsorption and Cell Infiltration in Nanofibrous Scaffolds." *Biomaterials* 33.12 (2012): 3428-445.

[48] Cardinali, Massimo, F. James Kratochvil, John F. Ensley, Keith C. Robbins, and W. Andrew Yeudall. "Functional Characterization in Vivo of Mutant P53 Molecules Derived from Squamous Cell Carcinomas of the Head and Neck." *Molecular Carcinogenesis* 18.2 (1997): 78-88. Web.

[49] Sell, Scott A. "Scaffold Permeability as a Means to Determine Fiber Diameter and Pore Size of Electrospun Fibrinogen."*Http://scholarscompass.vcu.edu/etd*. Biomedical Engineering and Bioengineering Commons, 2006. Web.

[50] Lamouille, Samy, Jian Xu, and Rik Derynck. "Molecular Mechanisms of Epithelial mesenchymal Transition." *Nature Reviews Molecular Cell Biology* 15 (2014): 178+.

Appendix A

Statistical Analysis of

Experimental Data

Figure 3.6 Fiber Widths

One Way Analysis of Variance

Raw Data:

Small (55 mg/ml)	Medium (115 mg/ml)	Large (180 mg/ml)
0.468	1.600	5.906
0.317	1.769	5.637
0.516	1.684	5.780
0.726	1.765	4.368
0.326	1.915	6.039
0.392	1.766	5.515
0.277	1.698	4.915
0.620	1.817	5.670
0.435	1.882	5.639
0.709	1.698	5.586
0.392	1.770	5.657
0.601	1.876	5.997
0.496	1.897	5.997
0.653	2.012	4.648
0.365	1.746	4.910
0.532	1.156	4.331
0.404	1.765	
0.594	1.471	6.395
0.675	1.475	6.067
0.351	1.593	6.981
0.577	2.095	6.119
0.387	1.897	
0.439	1.860	2.725
0.387	1.832	8.216
0.369	2.085	4.678
0.351	1.648	6.468
0.346	1.710	4.693
0.697	1.749	4.233
0.439	1.789	7.341
0.231	1.886	4.114
0.238	1.294	6.277

0.516	1.824	4.840
0.408	2.527	7.927
0.465	1.656	3.014
0.752	1.786	6.274
0.416	2.014	1.849
0.923	2.039	5.195
0.476	1.746	5.165
0.588	1.618	5.080
0.739	1.958	4.346
0.658	1.749	4.682
1.168	2.611	4.666
0.490	1.664	4.134
0.294	2.584	3.656
0.516	1.295	4.396
0.695	1.615	6.534
0.404	1.648	4.547
0.547	1.626	5.170
0.547	1.890	6.242
0.496	1.250	4.873
0.588	1.153	4.338
0.469	1.462	3.887
0.231	1.438	5.023
0.430	1.905	5.628
0.673	1.334	5.615
0.430	1.350	4.895
0.586	1.790	5.019
0.560	1.006	5.392
0.392	0.925	5.242
0.463	1.688	4.692
0.306	1.462	
0.731	1.294	4.507
0.361	1.472	4.900
0.350	1.739	4.649
0.484	1.334	6.915
0.361	1.463	4.782
0.478	1.676	5.221
0.391	1.575	5.109
0.471	1.336	6.926
0.316	1.575	5.181
0.423	1.732	5.631
0.416	2.000	5.670
0.409	1.821	5.072
0.470	1.298	5.713
0.509	1.789	5.637
0.385	1.036	6.360
0.587	1.239	4.835
0.532	1.996	4.942
0.196	1.736	3.565
0.611	1.517	6.039
0.532	1.074	2.278
0.416	1.745	2.031
0.438	1.654	7.859

0.525	1.520	4.770
0.637	1.705	6.697
0.597	1.360	5.386
0.334	1.206	4.550
0.316	1.849	5.396
0.596	1.617	5.179
0.476	1.705	3.923
0.471	1.965	4.442
0.282	1.720	4.638
0.554	2.113	2.771
0.385	1.708	4.991
0.527	1.241	2.735
0.582	1.947	4.225
0.238	1.491	5.662
0.532	1.648	5.830
0.385	1.390	6.731
0.473	1.754	4.680

Table Analyzed	Data 1
Kruskal-Wallis test	
P value	< 0.0001
Exact or approximate P value?	Gaussian Approximation
P value summary	***
Do the medians vary signif. (P < 0.05)	Yes
Number of groups	3
Kruskal-Wallis statistic	262.0

Number of values	100	100	97
Minimum	0.1960	0.9250	1.849
25% Percentile	0.3855	1.471	4.594
Median	0.4705	1.705	5.109
75% Percentile	0.5808	1.830	5.805
Maximum	1.168	2.611	8.216
Mean	0.4831	1.669	5.151
Std. Deviation	0.1517	0.3049	1.181
Std. Error	0.01517	0.03049	0.1199
Lower 95% CI	0.4530	1.608	4.913
Upper 95% CI	0.5132	1.729	5.389

Figure 3.7 Mechanical Testing of Scaffolds

One Way Analysis of Variance

(A) Average Thickness

Small (55 mg/ml)	Medium (115 mg/ml)	Large (180mg/ml)
0.0050	0.0050	0.0165
0.0045	0.0070	0.0165
0.0030	0.0065	0.0165
0.0030	0.0095	0.0165
0.0025	0.0075	0.0165
0.0035	0.0085	0.0165
0.0005	0.0070	
0.0005	0.0065	
0.0005	0.0065	

Table Analyzed	Data 1		
One-way analysis of variance			
P value	< 0.0001		
P value summary	***		
Are means signif. different? (P < 0.05)	Yes		
Number of groups	3		
F	199.7		
R squared	0.9501		
Bartlett's test for equal variances			
Bartlett's statistic (corrected)			
P value			
P value summary	ns		
Do the variances differ signif. (P < 0.05)	No		
ANOVA Table	SS	df	MS
Treatment (between columns)	0.0007059	2	0.0003529
Residual (within columns)	0.00003711	21	0.000001767
Total	0.000743	23	

Number of values	9	9	6
Minimum	0.0005	0.0050	0.0165
25% Percentile	0.0005	0.0065	0.0165
Median	0.0030	0.0070	0.0165
75% Percentile	0.0040	0.0080	0.0165
Maximum	0.0050	0.0095	0.0165
Mean	0.002556	0.007111	0.0165
Std. Deviation	0.001722	0.001294	0.0
Std. Error	0.0005740	0.0004312	0.0
Lower 95% CI	0.001232	0.006117	0.0165
Upper 95% CI	0.003879	0.008106	0.0165

(B.) Peak Stress

Small (55 mg/ml)	Medium (115 mg/ml)	Large (180 mg/ml)
2.638	3.714	1.966
2.536	3.591	1.219
2.752	3.867	1.641
3.297	4.521	1.276
5.646	2.368	1.747
3.492	2.468	1.562
9.679	3.621	
10.146	3.512	
9.743	2.546	

Table Analyzed	Data 1		
One-way analysis of variance			
P value	0.0063		
P value summary	**		
Are means signif. different? (P < 0.05)	Yes		
Number of groups	3		
F	6.511		
R squared	0.3827		
Bartlett's test for equal variances			
Bartlett's statistic (corrected)	27.98		
P value	< 0.0001		
P value summary	***		
Do the variances differ signif. (P < 0.05)	Yes		
ANOVA Table	SS	df	MS
Treatment (between columns)	59.02	2	29.51

Residual (within columns)	95.19	21	4.533
Total	154.2	23	

Number of values	9	9	6
Minimum	2.536	2.368	1.219
25% Percentile	2.695	2.507	1.262
Median	3.492	3.591	1.602
75% Percentile	9.711	3.791	1.802
Maximum	10.15	4.521	1.966
Mean	5.548	3.356	1.569
Std. Deviation	3.363	0.7346	0.2839
Std. Error	1.121	0.2449	0.1159
Lower 95% CI	2.963	2.792	1.271
Upper 95% CI	8.133	3.921	1.866

(C.) Strain At Break

Small (55 mg/ml)	Medium (115 mg/ml)	Large (180mg/ml)
0.229	0.214	2.952
0.266	0.184	2.470
0.190	0.268	3.218
0.217	0.221	2.541
0.320	0.171	2.410
0.274	0.141	3.072
0.329	0.154	
0.209	0.195	
0.351	0.142	

Table Analyzed	Data 1
Kruskal-Wallis test	
P value	0.0002
Exact or approximate P value?	Gaussian Approximation
P value summary	***
Do the medians vary signif. (P < 0.05)	Yes
Number of groups	3
Kruskal-Wallis statistic	16.83

Number of values	9	9	6

Minimum	0.1900	0.1410	2.410
25% Percentile	0.2130	0.1480	2.455
Median	0.2660	0.1840	2.747
75% Percentile	0.3245	0.2175	3.109
Maximum	0.3510	0.2680	3.218
Mean	0.2650	0.1878	2.777
Std. Deviation	0.05805	0.04183	0.3455
Std. Error	0.01935	0.01394	0.1410
Lower 95% CI	0.2204	0.1556	2.415
Upper 95% CI	0.3096	0.2199	3.140

Figure 3.8 Pore Size and Porosity

One Way Analysis of Variance

(A) Average Area of Pores

Small (55 mg/ml)	Medium (115 mg/ml)	Large (180 mg/ml)
3.105	5.778	6.555
3.397	5.032	3.683
	8.725	6.309
2.254	6.954	9.538
1.453	5.857	5.673
2.365	6.429	6.260
2.697	6.962	3.227
2.569	4.971	4.363
3.266	7.315	6.614
3.727	7.574	8.195
2.672		

Table Analyzed	Data 1		
One-way analysis of variance			
P value	< 0.0001		
P value summary	***		
Are means signif. different? (P < 0.05)	Yes		
Number of groups	3		
F	22.83		
R squared	0.6284		
Bartlett's test for equal variances			
Bartlett's statistic (corrected)	9.030		
P value	0.0109		
P value summary	*		
Do the variances differ signif. (P < 0.05)	Yes		
ANOVA Table	SS	df	MS

Treatment (between columns)	85.37	2	42.68
Residual (within columns)	50.48	27	1.870
Total	135.8	29	

10	10	10
1.453	4.971	3.227
2.337	5.592	4.193
2.685	6.692	6.285
3.299	7.380	7.009
3.727	8.725	9.538
2.751	6.560	6.042
0.6569	1.183	1.944
0.2077	0.3739	0.6147
2.281	5.714	4.651
3.220	7.406	7.432

(B) Porosity

Small (55 mg/ml)	Medium (115 mg/ml)	Large (180mg/ml)
52.5	44.2	24.0
53.9	41.3	23.8
	44.7	27.8
57.3	39.3	27.6
49.3	41.9	28.3
56.0	41.8	28.3
52.7	41.7	21.6
57.5	42.2	26.5
58.4	42.3	33.0
50.5	46.0	27.8
50.0		

Table Analyzed	Data 1
Kruskal-Wallis test	
P value	< 0.0001
Exact or approximate P value?	Gaussian Approximation
P value summary	***
Do the medians vary signif. (P < 0.05)	Yes
Number of groups	3
Kruskal-Wallis statistic	25.82

Number of values	10	10	10

Minimum	49.30	39.30	21.60
25% Percentile	50.38	41.60	23.95
Median	53.30	42.05	27.70
75% Percentile	57.35	44.33	28.30
Maximum	58.40	46.00	33.00
Mean	53.81	42.54	26.87
Std. Deviation	3.340	1.922	3.153
Std. Error	1.056	0.6079	0.9972
Lower 95% CI	51.42	41.16	24.61
Upper 95% CI	56.20	43.92	29.13